University of South-Eastern Norway
Faculty of Technology, Natural Sciences and Maritime Studies

Doctoral dissertation no. 38
2019

Marcus Sebastian Wild

Heat generation in underwater transducers

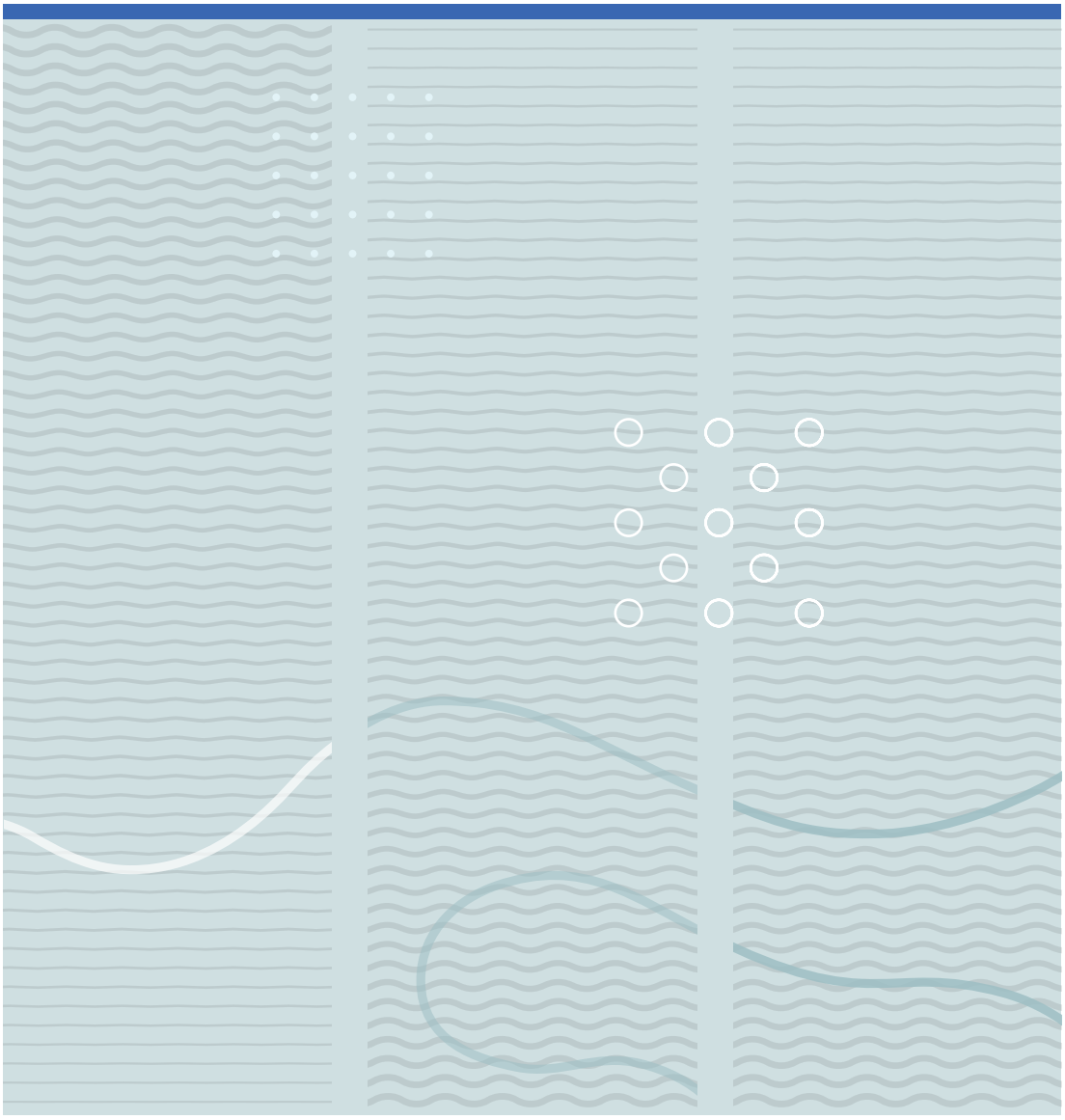

Marcus Sebastian Wild

Heat generation in underwater transducers

A PhD dissertation in
Applied Micro- and Nanosystems

Faculty of Technology, Natural Sciences and Maritime Studies
University of South-Eastern Norway
Horten, 2019

Doctoral dissertations at the University of South-Eastern Norway no. 38

ISSN: 2535-5244(print)
ISSN: 2535-5252 (online)

ISBN:978-82-7860-380-2 (print)
ISBN: 978-82-7860-381-9 (online)

Print: University of South-Eastern Norway

Acknowledgements

I would like to acknowledge my supervisors Karina Hjelmervik, Lars Hoff and Martin Bring for their guidance, help and encouragement throughout my PhD. They were particularly good at providing a supportive environment as well as letting me indulge in my favourite Norwegian past times: skiing, camping and hiking. I would also like to thank the co-authors Einar Halvorsen and Thong Huynh for their valuable input. I had the pleasure of supervising two Master's students during my PhD, Amirfereydoon Mansoori and Lars-Erik Myrstuen. I would like to thank them for the energy they put into their projects and for pushing my knowledge in the field of piezoelectricity. Finally, I wish to thank my family, my girlfriend and her family for their support during the PhD project.

Abstract

Acoustic transducers are used for a variety of applications, ranging from medical to maritime uses. In the maritime sector, underwater transducers can be used for applications such as seabed mapping, fishing and communication. Significant strides have been made in each of these applications, resulting in high performance transducers. However, as these transducers are being used with increasingly higher power, duty cycles and wider bandwidth, the heat generation within these systems has become an important design criteria. Indeed, it is clear that excessive temperatures can cause damage to underwater transducers.

One of the key contributors to the energy dissipation in underwater transducers is the active part, namely the piezoelectric material. The thesis concentrates on predicting the energy dissipation in a piezoelectric rod given known external conditions such as driving voltage and frequency of operation. To achieve this, the work initially focused on developing a characterisation method to characterise the relevant piezoelectric constants based on a global optimisation algorithm and a 1D or 3D FEM model. It was found that the piezoelectric loss, a parameter normally considered negligible, was an independent parameter which could be estimated through the developed characterisation method. In addition to this finding, it was shown the use of two cost functions in the global optimisation algorithm could negate the effects of noise on the characterised material constants. Finally, a local optimisation algorithm was used instead of a global optimisation algorithm to demonstrate that these types of methods can converge to local minima without adequate initial material constants.

The next step of the PhD was to predict the power dissipation density in the piezoelectric rod given the characterised material parameters. The initial goal was

to quantify the contribution from the mechanical, electrical and piezoelectric losses to determine whether the piezoelectric loss is indeed negligible. However, the most significant finding of this step was that the mechanical, electrical and piezoelectric contributions changed depending on the piezoelectric constitutive form used. This demonstrates that although the losses are associated with a specific mechanism under Holland's notation, such as mechanical, electrical and piezoelectric energy dissipation, they are in fact not associated directly with the physical energy dissipation mechanisms and must not be treated in this manner. This finding is emphasised by the fact that the contribution to the power dissipation from the imaginary part of the piezoelectric constant is negative. In addition, this study on the power dissipation in piezoelectric materials demonstrated that the loss parameters that originate from the BVD model should not be used as the loss parameters under Holland's notation as this results in a different power dissipation.

The final step of the PhD was to validate the temperature rise predicted from the characterised material parameters by comparing it to the measured temperature rise. This stage of the PhD found that the spatial distribution of the temperature rise across the length of the piezoelectric rod was better modelled by the predicted spatial distribution of the power dissipation density as opposed to a spatially constant power dissipation density. It also determined that from a practical point of view, using a power dissipation density that is constant in space was adequate for most purposes as the differences were not large.

List of papers

Papers 1, 2, 4 and 5 are omitted from online publication due to publishers restrictions.

This PhD thesis is based on the following articles:

Article 1

M. Wild, K. Hjelmervik, L. Hoff and M. Bring, "Characterising piezoelectric material parameters through a 3D FEM and optimisation algorithm," in OCEANS 2017 - Aberdeen, pp. 1-5, IEEE, 2017, doi: 10.1109/OCEANSE.2017.8084983

Article 2

This article is an extension of article 1, but the methods used are different enough to include article 1 in this list.

M. Wild, M. Bring, L. Hoff and K. Hjelmervik, "Characterization of Piezoelectric Material Parameters Through a Global Optimization Algorithm", IEEE Journal of Oceanic Engineering, pp. 1-9,, 2019, doi: 10.1109/JOE.2018.2882262

Article 3

M. Wild, M. Bring, E. Halvorsen, L. Hoff and K. Hjelmervik, "The challenge of distinguishing mechanical, electrical and piezoelectric losses," Journal of Acoustical Society of America, 144(4), pp. 2128-2134, 2018, doi: 10.1121/1.5057443

Article 4

M. Wild, M. Bring, L. Hoff and K. Hjelmervik, "Comparison of two models for power dissipation and temperature in piezoelectric transducers," in 2018 IEEE International Ultrasonics Symposium (IUS), pp. 1-4, IEEE, 2018, doi: 10.1109/ULT-

SYM.2018.8580069

Article 5

M. Wild, T. Huynh, M. Bring, L. Hoff and K. Hjelmervik, "Estimating the spatial temperature distribution in a piezoelectric rod," submitted to IEEE Transactions on Ultrasonics, Ferroelectrics and Frequency Control, pp. 1-7, 2019

Co-Author of the following publications:

This article was not included in the thesis.

Article 6:

A. Mansoori, M. Wild and L. Hoff, "A FEM-based Method for Complete Parameter Identification of Thin Piezoceramic Bars," 2018 IEEE Ultrasonics Symposium, Kobe, Japan, 2018

List of Figures

Abbreviations

1D ..... One-Dimensional

3D ..... Three-Dimensional

BVD ..... Butterworth Van Dyke

FEM ..... Finite-Element-Method

KLM ..... Krimholtz-Leedom-Matthaei

PZT ..... Lead Zirconate Titanate

SONAR ..... Sound Navigation Ranging

List of Symbols

C_0 ..... Static Capacitance

C_1 ..... Motional Capacitance

L_1 ..... Motional Inductance

R_1 ..... Motional Resistance

f_r ..... Resonance Frequency

f_1, f_2 ..... Half-power Frequencies

Contents

Chapter 1

Introduction and Background

1.1 Background

Underwater acoustic transducers are in use in many maritime sectors such as fishing, oil and gas and defence. The acoustic transducer industry has continuously been improving the performance of these instruments in order to adapt to the ever increasing demands of the applications. This has resulted in underwater transducers that can operate with increasingly higher duty cycles, bandwidths and power.

Figure 1.1: Two examples of underwater transducers used in maritime industries. Pictures taken from Kongsberg Maritime website.

Although all of these improvements have resulted in higher performance transducers, this has also affected the amount of power that is dissipated by the transducer. Indeed, increasing the duty cycle gives the transducer less time to cool down.

Increasing the power means that a higher amount of power is also dissipated. This will cause the transducer to heat up, significantly in some cases. The result is that some high performance transducers may not be able to operate at the highest desired power in order to limit the heat generation [2, 3].

High temperatures within the transducer can affect the integrity of the structure and materials within. Indeed, the various layers can start to delaminate in a transducer given high temperatures [4]. It may also cause premature ageing of the materials in the transducer [5, 6]. The materials inside the transducer have temperature dependent material properties, and therefore operating the transducer at higher temperatures may change the behaviour of the transducer away for the original design objectives. Indeed, studies have quantified the temperature dependency of the piezoelectric material [7, 8].

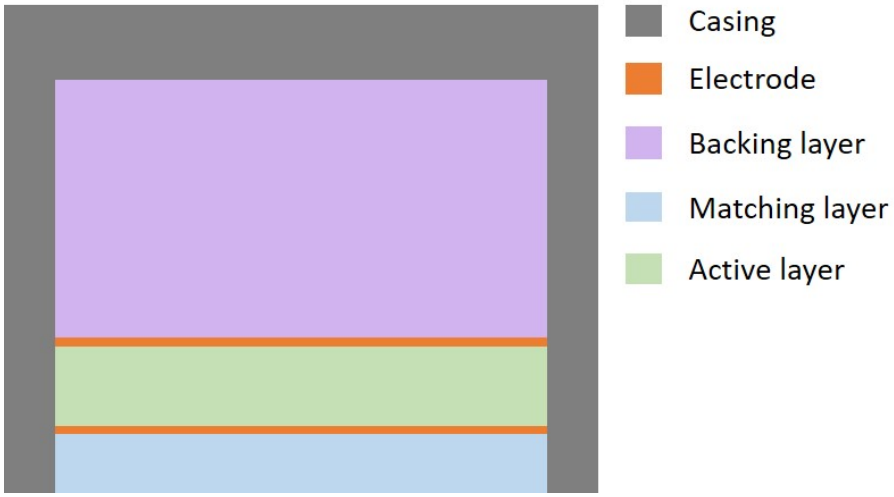

Figure 1.2: Simplified schematic of a transducer. The active layer can either be a piezoelectric material or a composite.

The power dissipation in the materials in a transducer originates from the inherent energy loss mechanisms in these materials, shown in Fig. 1.2. This is called the mechanical loss in the passive mechanical materials such as the matching and backing layer. In the electrodes and other electrical components, there is also a dielectric loss. In the active layer of the transducer, the piezoelectric material has three loss mechanisms that are commonly named the mechanical, dielectric and piezoelectric loss. This makes the piezoelectric component more complicated to characterise, as the mechanisms are interlinked. The piezoelectric material can be a significant

contributor to the total power dissipation in the active layer [9].

1.2 Previous work on heat generation in transducers

As heat generation can limit the performance of high power transducers, it is a subject that has received attention in the literature for medical, non destructive testing and underwater transducers. Abboud et al., recognising that thermal management in high power transducers was an important aspect of the design process, modelled the temperature rise in an underwater transducer under different conditions [10]. One of the main conclusions from that study was that the quality of the temperature prediction required accurate characterisation of the material parameters. In the medical transducer industry, the maximum temperature the surface of an ultrasound probe can reach is strictly regulated to protect the patient from harm. Studies have focused on predicting the temperature rise specifically at the surface of the transducer [11, 12, 13, 14].

Researchers have investigated different techniques to mitigate the problems associated the temperature rise within the transducer. Part of the research has focused on using materials that reduce the power dissipation in the transducer whilst maintaining the performance [15, 2]. Other studies have focused on using materials that stay stable as the temperature increases. Hollenstein et al. used modified materials for medical transducers that stayed stable even with repeated temperature cycling due to sterilisation demands [16]. Finally, Hirose et al. have shown that for the same vibration velocity, the efficiency of the piezoelectric material was higher at the antiresonance than at the resonance frequency due to lower losses at higher powers [17]. This should result in a lower temperature rise for the same acoustic performance.

1.3 Research Goals and Approach

As the piezoelectric material is an important contributor to the power dissipation in underwater transducers, the PhD focused on the piezoelectric component. The aim of this PhD was to determine whether the spatially dependent power dissipation density in a piezoelectric material, for known operational conditions, could be sufficiently accurately predicted given a robust characterisation method. If successful, this would be the first step to ensure that the temperature rise could be accurately predicted in a model for a particular transducer design. Thus, the thermal performance of the underwater transducer could be taken into account as a design criterion. This would also enable the design of a high power transducer to be optimised to maximise performance whilst minimising the temperature rise.

The approach taken in the PhD was to initially set up a robust characterisation method to characterise the important material parameters that govern the power dissipation in a piezoelectric material. As the transducer of interest in the case of this PhD has a 1-3 composite as the active layer, shown in Fig 1.3, the particular shape of interest is a piezoelectric rod excited in the length extensional mode. This characterisation method was developed as the IEEE Standard on Piezoelectricity characterisation method [18] does not take into account the piezoelectric loss parameter. Multiple studies on this subject showed that accurately characterising these material parameters, including the piezoelectric loss, was important in order to accurately predict the power dissipation in a piezoelectric material. Furthermore, the characterisation method was also developed to understand the dependency the material parameters, and therefore the power dissipation, have on external effects such as the driving voltage or temperature. Indeed, this thesis shows the temperature and driving voltage dependency of the piezoelectric material parameters.

The second stage of the PhD project was to model the spatially and frequency dependent power dissipation density in a piezoelectric rod, given the material properties characterised in the first stage. This was achieved through the use of a 1D Mason model and the power dissipation density as a result of the general Poynting vector for piezoelectric materials. Given the electric and mechanical fields predicted in a 1D Mason model, the power dissipation density can be calculated using the

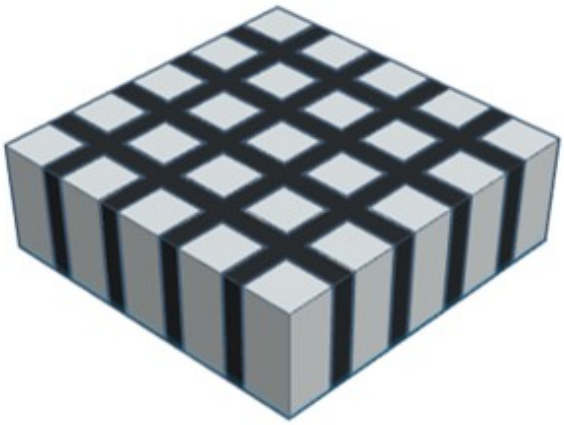

Figure 1.3: Simplified schematic of a 1-3 composite where the grey material is the piezoelectric material and the surrounding black material is made of epoxy.

divergence of the general Poynting vector. The divergence of the general Poynting vector results in an equation with three terms which have been previously named the mechanical, dielectric and piezoelectric contribution to the power dissipation density. One of the goals of this second stage was initially to quantify the importance of these different contributions to the total power dissipation. However, it was shown that distinguishing between a mechanical, dielectric and piezoelectric contribution to the power dissipation does not hold when considering physical mechanisms within the piezoelectric material. This was demonstrated by comparing the mechanical, dielectric and piezoelectric contributions to the total power dissipation for different piezoelectric constitutive forms.

The final stage of the PhD project was to verify the spatially dependent temperature rise in a piezoelectric rod given the predicted spatially dependent power dissipation density from the previous stage. To achieve the goal of this stage, the temperature profile along the length of a piezoelectric rod was measured with thermocouples placed on the surface of the material. The temperature of the piezoelectric rod was then modelled in a 3D FEM model using the spatially dependent power dissipation density predicted from the previous stage. For comparison, the temperature of the piezoelectric rod was also modelled in a 3D FEM model using a spatially constant power dissipation density to determine the importance of the spatial dependence of the power dissipation density.

1.4 Impact of results

The intent of the first stage of the project was to determine the uniqueness of the piezoelectric loss as a parameter in the piezoelectric model. The developed characterisation method fits the predicted admittance spectrum from a 1D Mason model to the measured admittance curve of the sample of interest using an optimisation algorithm. The size of the search space of the piezoelectric loss parameter was kept deliberately large to test whether the parameter would converge to a meaningful value. Under these conditions, the piezoelectric loss parameter did converge to a specific value in the characterisation algorithm. Indeed, a sensitivity analysis showed that the cost function of the optimisation algorithm is sensitive to the piezoelectric loss. The impact of using different cost functions when using optimisation algorithms to characterise piezoelectric materials was analysed. For both the impedance and admittance based cost functions, the uncertainty of the characterised material parameters increased as the noise in the measured data increased. Noise at the antiresonance frequency in the measured admittance spectrum is a particular problem for high impedance samples, such as piezoelectric rods. However, the average of the estimated material parameters from the two cost functions for high levels of random noise remained close to estimated material parameters for low levels of noise. The use of two cost functions is therefore advantageous when the measured data has high levels of random noise.

The second stage of the PhD focused on quantifying the contributions to the power dissipation density in piezoelectric materials. In industry and in the literature, a significant amount of assumptions surround the importance of the mechanical, dielectric and piezoelectric loss in piezoelectric materials. It is common to ignore the piezoelectric loss as it is assumed to have a negligible effect on the power dissipation. There are also many assumptions surrounding the importance of the mechanical and dielectric loss at the resonance and antiresonance frequency. However, this project showed that the mechanical, electrical and piezoelectric contributions depend on the piezoelectric constitutive form used and therefore assumptions cannot be based on physical mechanisms in the piezoelectric material. This is emphasised by the fact that the piezoelectric contribution to the total power dissipation can be negative.

The impact of this result is to show that the mechanical, dielectric and piezoelectric loss should be viewed as macroscopic parameters in a model rather than be attached to physical mechanisms.

The predicted and measured spatially dependent temperature along the length of the piezoelectric rod was compared in the final stage of the PhD. Although there were some discrepancies in the match between the measured and modelled temperatures, the difference between the temperature rise at the edge and the centre of the rod matched well. This gives confidence that characterising the losses under Holland's representation of loss can be used to determine the spatial dependence of the power dissipation density in piezoelectric materials. The impact of this is that the spatial dependence of the temperature rise in a piezoelectric material can be predicted by accurately characterising the material parameters.

1.5 Structure of Thesis

The thesis is divided into five chapters. The first chapter gives background information on the motivation and impact of the PhD project. The second chapter introduces the theory of piezoelectricity and the different representations of losses in piezoelectric materials. This is followed by a short review of the characterisation methods currently in use in the literature. The chapter continues with an overview of the characterisation method developed in the PhD. The characterisation method detailed in this thesis was first documented in a conference paper [19] which was then extended into a journal article [20]. Finally, the chapter ends with some additional work on the temperature dependency of the piezoelectric material constants that was not published.

The third chapter introduces the theory of power dissipation density in piezoelectric materials calculated from the general Poynting vector. This is followed by a review of the studies that predict the power dissipation in piezoelectric materials. An overview of the second stage of the PhD project which focused on the power dissipation density in the piezoelectric rod is then given. This work was published in a journal article [21]. A comparison of the power dissipation density in a transducer as a result of Holland's representation and the IEEE Standard on Piezoelectricity

representation of loss is then described [22].

The fourth chapter introduces previous studies on the measurement and modelling of the temperature rise in piezoelectric materials. This is followed by an overview of the work from the third stage of the PhD on the prediction of the spatially dependent temperature rise in a piezoelectric rod, which was submitted as a journal article.

The final chapter concludes the thesis. An overview of the important results is given followed by suggestions for future work on the subject.

Chapter 2

Characterisation of piezoelectric materials

In order to predict the power dissipation in a piezoelectric rod, accurate material parameters were needed. In the initial stages of the PhD, it was clear that the material parameters provided by the piezoelectric manufacturer were not accurate enough. The reasons for this lack of accuracy could be due to the material having been characterised at a different frequency. Another cause could be the effect the dicing process has on the material properties. Therefore, a characterisation method was developed to determine the parameters more accurately. A characterisation method would also be invaluable to determine the driving voltage and temperature dependency of the piezoelectric material parameters. An additional goal of the characterisation method was to determine the uniqueness of the imaginary part of the piezoelectric constant, also known as the piezoelectric loss. Indeed, it is common to neglect this parameter as it is assumed to be negligible or non-unique. This chapter will first give an overview of piezoelectric theory. This will be followed by a brief overview of the physical mechanisms that are thought to be responsible for the energy loss in piezoelectric materials. Then, the different representations of loss used in the industry and literature will be described. Following on from this, the characterisation method and the subsequent results, detailed in two of the articles [19, 20], will be described. Finally, a final section will give an overview of the calculated temperature dependency of the piezoelectric material parameters

estimated from the developed characterisation method as well as the results of the characterisation method when neglecting the piezoelectric loss.

2.1 Piezoelectric theory

The project concentrated solely on piezoelectric materials made from lead zirconate titanate, or PZT as it is more commonly known. This material has ∞m type symmetry, which greatly reduces the number of material parameters. For such a material, the governing equations that determine the relationship between the stress, strain, electric field and electric displacement field are called the piezoelectric constitutive equations and are given here:

$$\begin{aligned} \boldsymbol{S} &= \boldsymbol{s^D T} + \boldsymbol{g}^t \boldsymbol{D}, \\ \boldsymbol{E} &= -\boldsymbol{g T} + \boldsymbol{\beta^T D}, \end{aligned} \tag{2.1}$$

where $\boldsymbol{S}$ is the strain tensor, $\boldsymbol{T}$ is the stress tensor, $\boldsymbol{E}$ is the electric field vector, $\boldsymbol{D}$ is the electric displacement vector, $\boldsymbol{s^D}$ is the elastic compliance tensor at constant electric displacement field, $\boldsymbol{g}$ is the piezoelectric constant tensor, $\boldsymbol{\beta^T}$ is the electric impermittivity tensor at constant stress and t denotes the transpose. The temperature dependence of the piezoelectric constitutive equations is carried by these material constants.

The PhD focused on 1-3 composite structures that is composed of piezoelectric rods polarised along the length axis as shown in Fig. 2.1. This structure has a length extensional mode, which is the mode used in 1-3 composites. The length extensional mode in a long piezoelectric rod can be treated as a 1D problem by assuming that $T_1 = T_2 = 0$, $E_1 = E_2 = 0$, $D_1 = D_2 = 0$ and $\frac{dD_3}{dx_3} = 0$ near the resonance frequency. If the shear stress and strains are then also omitted, Eq. 2.1 is then reduced to

$$\begin{aligned} S_3 &= s_{33}^D T_3 + g_{33} D_3, \\ E_3 &= -g_{33} T_3 + \beta_{33}^T D_3, \end{aligned} \tag{2.2}$$

where the 33 subscripts indicate the $(3,3)$ tensor indices. This can also be transformed to the d-form of the piezoelectric constitutive equations as

$$\begin{aligned} S_3 &= s_{33}^E T_3 + d_{33} E_3, \\ D_3 &= d_{33} T_3 + \varepsilon_{33}^T E_3, \end{aligned} \tag{2.3}$$

where s_{33}^E is the elastic compliance at constant electric field, d_{33} is the piezoelectric constant, ε_{33}^T is the relative electric permittivity at constant stress.

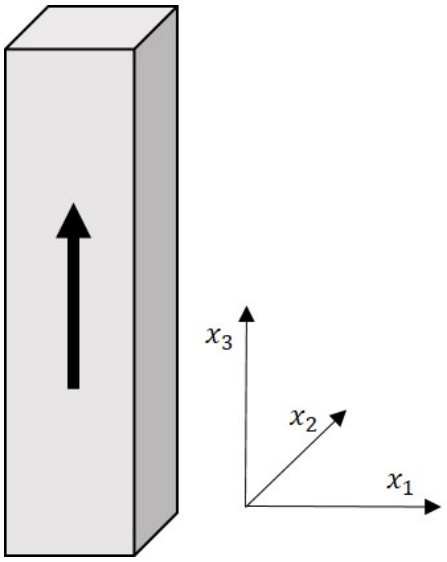

Figure 2.1: A piezoelectric rod polarised in the direction of the bold arrow.

2.2 Physical processes of losses in piezoelectric materials

The physical processes that govern energy loss in piezoelectric ceramics is typically separated into two categories: intrinsic and extrinsic losses [23]. Intrinsic losses are associated with lattice deformation of the unit cell. An example of an intrinsic effect is the deformation of the lattice through an external electric field which causes the polarisation of a unit cell to reorient itself in a different direction. Although piezoelectric materials that can easily change the polarisation direction have enhanced piezoelectric properties, they also exhibit higher energy loss. This would suggest that there is a loss mechanism associated with reorientation of the polarisation direction under an electric field. Extrinsic losses are due to energy loss originating from phenomenons on a larger scale such as domain wall motion. Domain walls are the boundaries between two electrical domains with different polarisation directions

in a piezoelectric material. Under an applied electric field, these domain walls will move, but with a delayed response thus causing a hysteretic response. This causes extrinsic energy loss in the piezoelectric material.

2.3 Representations of loss in piezoelectric models

There are different representations of loss in use for piezoelectric materials. The simplest and one of the most common representations for losses in piezoelectric materials originates from lumped models such as the BVD model. Another common representation is the one introduced by Holland which is applicable for distributed models such as the 1D Mason or 3D FEM model [24]. Finally, less common representations of loss use established viscoelastic models such as the Zener or Debye model which can give an insight into the physical mechanisms of energy loss in the piezoelectric material.

2.3.1 Lumped losses

The most common representation of loss in piezoelectric materials is through two material parameters called the mechanical quality Q_m and dielectric loss $\tan(\theta)$. These parameters can be introduced into the Butterworth-Van-Dyke (BVD) equivalent circuit of a piezoelectric material (Fig. 2.2). The BVD equivalent circuit is considered to be a lumped model of the piezoelectric material. This is the representation that is used to characterise piezoelectric materials in the IEEE Standard on Piezoelectricity [18].

The mechanical quality Q_m can be determined by measuring the sharpness of the resonance in the measured admittance curve as shown in Fig. 2.3, with

$$Q_m = \frac{f_r}{f_2 - f_1}, \tag{2.4}$$

where f_r is the resonance frequency and f_1 and f_2 are the frequencies at which the value of the admittance is 3 dB less than the value of the admittance at f_r. This

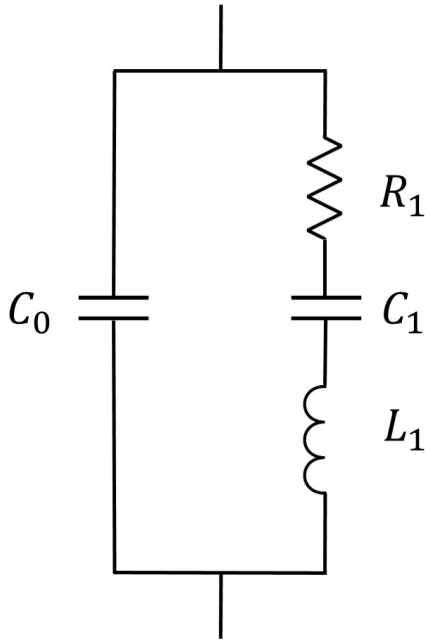

Figure 2.2: The BVD model for a piezoelectric material. The branch on the right is called the motional branch whilst the branch on the left is called the static branch.

can also be determined through the BVD model using the following relationship between the mechanical quality and the components of the motional branch:

$$Q_m = \frac{(L_1/C_1)^{1/2}}{R_1}. \tag{2.5}$$

The dielectric loss $\tan(\theta)$ is typically determined by measuring the capacitance of the piezoelectric material away from the resonance frequency. This can either be at a low frequency or at a high frequency. In the IEEE Standard on Piezoelectricity, the dielectric loss is determined at a low frequency, and is therefore implemented as the imaginary part of the electric permittivity at constant stress. For a piezoelectric rod excited in the length extensional mode, the electric permittivity at constant stress, ε_{33}^T, becomes

$$\varepsilon_{33}^T = \varepsilon_{33}^T{}'(1 - j\tan(\theta)). \tag{2.6}$$

This parameter can then used as the electric permittivity for the static capacitance C_0 shown in the static branch of Fig. 2.2.

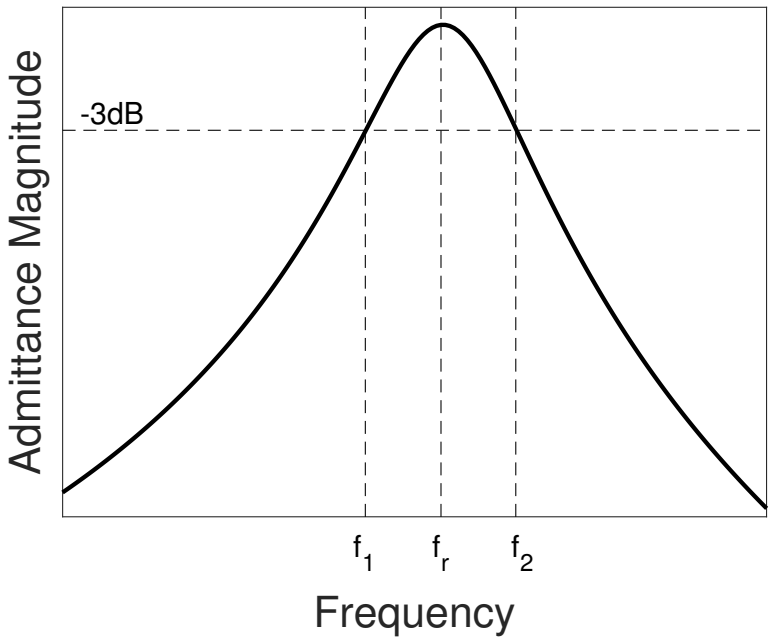

Figure 2.3: The method for determining the mechanical quality using the measured admittance curve at the resonance frequency.

2.3.2 Holland's representation of loss

For distributed models such as the Mason model or Finite-Element-Method (FEM) models, it is typical to use Holland's representation of loss [24]. Using Uchino and Hirose's notation [25], the material parameters are considered complex under this representation and are defined as

$$\begin{aligned} \boldsymbol{s}^{\boldsymbol{E}} &= \boldsymbol{s}^{\boldsymbol{E}\prime}(1 - j\tan\phi), \\ \boldsymbol{\varepsilon}^{\boldsymbol{T}} &= \boldsymbol{\varepsilon}^{\boldsymbol{T}\prime}(1 - j\tan\theta), \\ \boldsymbol{d} &= \boldsymbol{d}'(1 - j\tan\delta), \end{aligned} \tag{2.7}$$

where $\boldsymbol{s}^{\boldsymbol{E}\prime}$ is the real part of the complex elastic compliance tensor at constant electric field, $\boldsymbol{\varepsilon}^{\boldsymbol{T}\prime}$ is the real part of the complex relative electric permittivity tensor at constant stress, $\boldsymbol{d}'$ is the real part of the complex piezoelectric constant tensor, $\tan\phi$ is the mechanical loss tangent, $\tan\theta$ is the dielectric loss tangent and $\tan\delta$ is the piezoelectric loss tangent. In this case, the losses are considered isotropic and are therefore scalars. However, the losses are in reality anisotropic and can also be

represented as tensors to reflect this.

Given the 1D assumptions for a piezoelectric rod introduced in Section 2.1, Eq. 2.7 simplifies to

$$\begin{aligned} s_{33}^{E} &= s_{33}^{E\prime}(1 - j\tan\phi), \\ \varepsilon_{33}^{T} &= \varepsilon_{33}^{T\prime}(1 - j\tan\theta), \\ d_{33} &= d'_{33}(1 - j\tan\delta), \end{aligned} \tag{2.8}$$

where $s_{33}^{E\prime}$ is the real part of the elastic compliance at constant electric field, d'_{33} is the real part of the piezoelectric constant, $\varepsilon_{33}^{T\prime}$ is the real part of the relative electric permittivity at constant stress.

2.3.3 Other representations of loss

There are disadvantages to using the lumped loss model and Holland's representation of loss. Indeed, these representations are only valid over a limited range of frequencies and do not take into account the frequency dependent nature of attenuation in piezoelectric materials. They are also acausal, the behaviour of the material depends on the future, which means that these models may not represent physical mechanisms. Other models such as the Zener model, also known as the Debye model, are an initial step to overcome these issues. Powell et al. characterised a piezoelectric material at different frequencies using Holland's representation and found that the Debye model fit well to the frequency dependent curve of the dielectric constants [26]. More complicated models known as fractional models have also been found to fit the frequency dependent curve of the piezoelectric constants very well [27]. The advantage of these models is that they can be used to interpret the physical processes underlying energy loss in piezoelectric materials. The disadvantage of these models is that they require more parameters to be characterised. This may not be practical for applications that are only interested in a limited range of the frequency spectrum.

2.4 Characterisation of piezoelectric materials in the literature

There are numerous methods described in the literature that characterise materials in different manners. Probably the most commonly used characterisation method is described by the IEEE Standard on Piezoelectricity [18]. This method, described briefly in section 2.3.1, uses impedance measurements of piezoelectric samples of different shapes to analytically determine the piezoelectric constants that govern the different resonance modes. By characterising piezoelectric materials of different shapes, the full material tensors can be determined. Generally, the piezoelectric material constants provided by the piezoelectric material manufacturers are determined using this method. Multiple studies use the IEEE Standard method and an impedance measurement to characterise the piezoelectric material constants, including the mechanical quality and dielectric loss [28, 29, 15].

The IEEE Standard method is an analytical method that characterises two loss mechanisms. In order to include the piezoelectric loss in the characterisation method, Sherrit et al. used complex material parameters in the 1D Mason and KLM models for the thickness mode to obtain a set of equations which can be used to determine the piezoelectric material constants in a similar manner to the IEEE Standard method [30]. This was generalised by Sherrit and Mukherjee to determine the material parameters, including the piezoelectric loss, for a variety of piezoelectric sample shapes with different resonance modes [31]. The importance of the piezoelectric loss was also recognised by Uchino and Hirose who developed an equivalent circuit that could take the piezoelectric loss into account [25]. This equivalent circuit was then generalised to determine the piezoelectric material constants, including anisotropic mechanical, dielectric and piezoelectric losses, for samples of different shapes [32].

The methods described so far have used analytical expressions to extract the material constants from a measured impedance curve. A different approach is to use an optimisation algorithm and a suitable model of the piezoelectric material to fit the modelled impedance curve to the measured impedance curve. Kwok et

al. developed a method based on the optimisation approach with a 1D model [33]. Using an optimisation algorithm approach also renders the use of numerical models, such as FEM models, to characterise piezoelectric materials possible. This approach has been documented in multiple studies [34, 35, 36, 37, 38]. The advantage of these methods is that the full piezoelectric material constants can be determined with less samples of different shapes than the analytical methods. However, Mansoori et al. found that some material constants were not identifiable when using only one sample [39]. The disadvantage is that these methods are computer intensive and can require a significant amount of iterations to determine so many parameters.

2.5 Outline of the characterisation method

2.5.1 Goals and Method

The characterisation method developed in this project was based on fitting the modelled impedance or admittance curve to the measured impedance or admittance curve by varying the material parameters using an optimisation algorithm. There are six material parameters to determine based on Eq. 2.8. One of these material parameters is the imaginary part of the piezoelectric constant, also known as the piezoelectric loss. In many studies, the piezoelectric loss is normally considered to either be negligible or not an independent parameter. Therefore, one of the goals was to determine whether the characterisation method could find a unique piezoelectric loss parameter. A global optimisation algorithm was used to find the correct material parameters. The impedance of the piezoelectric rod is measured using an impedance analyser. The modelled admittance was initially calculated using a FEM model of the piezoelectric rod in COMSOL and the global optimisation algorithm used was simulated annealing [19]. The optimisation algorithm fits the modelled curve to the measured curve by minimising the cost function which is given by

$$C_Y = \sqrt{\frac{1}{M}\sum_{m=1}^{M}\left|\frac{Y_{mea}(m) - Y_{mod}(m)}{Y_{mea}(m)}\right|^2}, \tag{2.9}$$

where $Y_{mea}(m)$ and $Y_{mod}(m)$ are the discrete measured and the discrete modelled complex electrical admittances and M is the number of sample points.

It was found that using a FEM model in this method was computer intensive and algorithms such as simulated annealing require a significant amount of iterations to reach a solution. Studies mentioned in section 2.4 that use FEM models to characterise the piezoelectric material used local optimisation algorithms, which need less iterations but can miss the global minimum. As one of the goals of this project was to understand whether the piezoelectric loss is unique, a global optimisation algorithm was necessary.

Therefore, in order to overcome these limitations, the FEM model was replaced with a 1D Mason model [20] (shown in Fig.2.4) and the simulated annealing solver was replaced with the scatter search and local nonlinear problem solver [40]. The 1D Mason model can take into account complex material parameters and is not computer intensive. For a piezoelectric rod excited in the length extensional mode, simplifying from a 3D to 1D model is valid and only has a small influence on the accuracy of the characterised material parameters. The scatter search and local nonlinear problem solver is not as robust as simulated annealing, but it is much faster at finding the global minimum for simple problems.

Characterisation of piezoelectric materials using this type of method can be achieved using cost functions based on the impedance, admittance or both. This study investigated whether there was any difference between using an impedance or admittance based cost function. The admittance based cost function is shown in Eq. 2.10 and the impedance based cost function is

$$C_Z = \sqrt{\frac{1}{M}\sum_{m=1}^{M}\left|\frac{Z_{mea}(m) - Z_{mod}(m)}{Z_{mea}(m)}\right|^2}, \tag{2.10}$$

where $Z_{mea}(m)$ and $Z_{mod}(m)$ are the discrete measured and the discrete modelled complex electrical impedances. It was also found that for piezoelectric rods, the admittance at the antiresonance frequency can be very low. This meant that the antiresonance peak tended to be affected by random noise, as shown in Fig. 2.5, which could affect the characterisation of the piezoelectric rod. The magnitude of the effect of random noise on the determined material parameter values was quantified

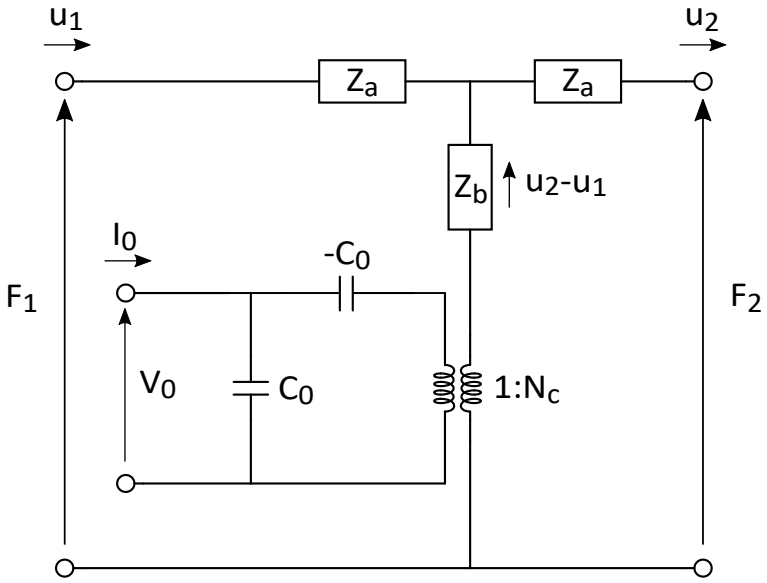

Figure 2.4: Mason 3-port equivalent circuit for the mechanical motion and electrical current of a piezoelectric rod following [1]. u_1 and F_1 are the velocity and force on the left surface, u_2 and F_2 the velocity and force on the right surface, and I_0 and V_0 the current and voltage at the electrical port.

in the study. In addition, the determined material parameters were compared to the material parameters determined using the IEEE Standard method. Finally, a local optimisation algorithm was used instead of the global optimisation algorithm to test whether a global algorithm is needed.

2.5.2 Results

The results of this study showed that the algorithm found a clear minimum for the piezoelectric loss (Fig. 2.6). This would suggest that it is an independent parameter in the model, even though the admittance is not as sensitive to this parameter as it is to the mechanical loss. The admittance and impedance cost functions found the same solution and showed similar sensitivity to the material parameters. However, with increasingly higher levels of random noise in the measured data, the estimated material parameters from the admittance and impedance based cost functions diverged from each other. Whilst the noise had a small influence on the real parts of the material constants, the effect was more pronounced for the loss components. Furthermore, whilst the solution from the impedance and admittance based cost

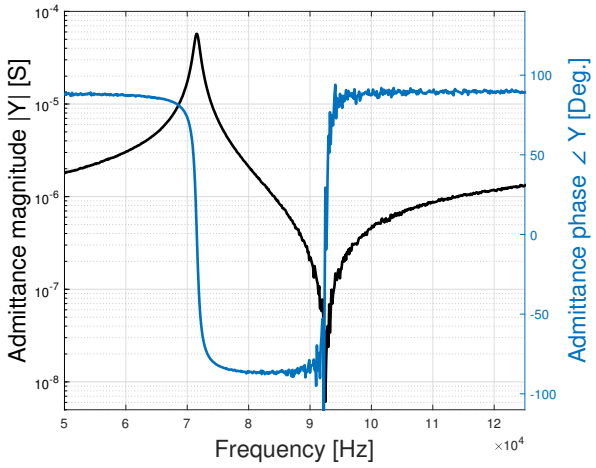

Figure 2.5: Admittance curve for piezoelectric rod. Note the noise at the antiresonance frequency.

functions diverged from each other, the average of the two solutions remained within a tolerable range of the original solution.

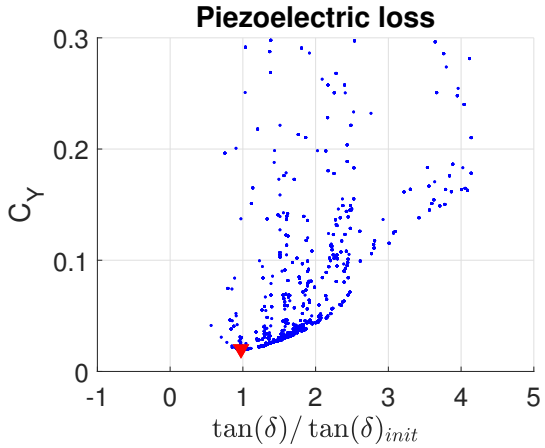

Figure 2.6: Admittance cost function C_Y value as a function of parameter value. The parameter values have been normalised with respect to the initial data a_{init}. All the local minima are represented by red triangles.

The determined materials parameters using this characterisation method were compared to those determined using the IEEE Standard method. Although the real part of the material constants were very comparable, the determined loss components were significantly different. It was also found that the IEEE Standard had higher standard deviations when the impedance measurement was repeated compared to the developed characterisation method.

Finally, the characterisation method converged to a local minimum when a local optimisation algorithm was used with the manufacturer data used as the initial point for the solver. If the material parameters determined by the IEEE Standard were chosen as initial parameters, the local optimisation algorithm converged to the global minimum. This shows that using a local optimisation algorithm can be disadvantageous as the initial points need to be chosen carefully.

2.6 Further unpublished work on characterisation

To further investigate the importance of the piezoelectric loss when characterising a piezoelectric material, the characterisation method was implemented without a piezoelectric loss. The determined material parameters as a result of removing the piezoelectric loss from the characterisation method are shown in Tab. 2.1. The cost function of the global minimum for the characterisation method without the piezoelectric loss is twice as large as the cost function value found in the characterisation method with the piezoelectric loss included. A higher cost function signifies that the modelled admittance curve does not fit as well to the measured admittance curve. Furthermore, the determined dielectric loss when the piezoelectric loss is not included is negative. This would result in a negative total power dissipation in the piezoelectric material and is therefore not a reasonable value [24].

Using such a characterisation method, the temperature dependence of the material parameters could be investigated. The impedance was measured on a piezoelectric rod placed in an oven at two different temperatures, 25°C and 50°C. The results of the characterisation are shown in Tab. 2.2. All of the material parameters increase from 25°C to 50°C. This is especially true for the loss components which increase by up to 25%. Understanding how the material parameters change with temperature is important for transducer designers as this can affect the performance and behaviour of the piezoelectric material.

Table 2.1: Comparison of determined material parameters with and without the piezoelectric loss included in the list of material parameters to determine in the characterisation method. The cost function value the minimum found is also shown.

Material Parameters	With piezoelectric loss	Without piezoelectric loss
$s_{33}^{E\prime}$ [$\times 10^{-12}\mathrm{m}^2/\mathrm{N}$]	17.18	17.19
$\varepsilon_{33}^{T\prime}$	1490.5	1487.5
d'_{33} [pC/N]	320.3	320.3
$\tan(\phi)$	0.0139	0.0125
$\tan(\theta)$	0.0154	-0.0201
$\tan(\delta)$	0.0195	0
C_Y	0.0201	0.0401

Table 2.2: Comparison of determined material parameters characterised at different temperatures.

Material Parameters	25°C characterisation	50°C characterisation
$s_{33}^{E\prime}$ [$\times 10^{-12}\mathrm{m}^2/\mathrm{N}$]	16.91	17.04
$\varepsilon_{33}^{T\prime}$	1730.1	1865.5
d'_{33} [pC/N]	320.1	335.8
$\tan(\phi)$	0.0123	0.0145
$\tan(\theta)$	0.0198	0.0245
$\tan(\delta)$	0.0205	0.0249

Chapter 3

Power dissipation in piezoelectric materials

Following on from the characterisation of a piezoelectric rod in the first chapter, the goal of this second stage was to model the power dissipation density in the piezoelectric rod. The power dissipation can be further investigated by quantifying the importance of the contributions from the characterised loss constants. This would determine whether the piezoelectric loss is negligible, as is commonly assumed, or whether it has an important contribution. Furthermore, it is shown that linking the imaginary part of the material constants, also known as the mechanical, dielectric and piezoelectric loss, to a physical process is not recommended [21]. This chapter starts by introducing the generalised Poynting vector, which is used to calculate the power dissipation density in a piezoelectric rod. This is followed by a review of previous studies on the subject of power dissipation in piezoelectric materials. Then, the power dissipation density in a piezoelectric material is modelled and its contributions are investigated [21]. The chapter concludes with a study on the consequences of mixing the IEEE Standard and Holland's representation of loss when considering power dissipation in a transducer.

3.1 Generalised Poynting Vector

The Generalised Poynting Vector is described by Holland [24] and Auld [41]. It is an amalgamation of the energy flux vector for mechanical and electromagnetic fields

and is given as

$$\mathbf{\Sigma} = \frac{1}{2}(\mathbf{E} \times \mathbf{H}^* - \mathbf{T} \cdot \mathbf{u}^*), \tag{3.1}$$

where $\mathbf{H}$ is the magnetic field, $\mathbf{u}$ is the particle velocity, * marks the complex conjugate and $\cdot$ is the inner product.

The power dissipation density for piezoelectric materials can be derived from Eq. 3.1 as

$$P = \frac{1}{2}\omega \mathrm{Im}(\mathbf{E} \cdot \mathbf{D}^* + \mathbf{T} : \mathbf{S}^*), \tag{3.2}$$

where P is the power dissipation density, ω is the angular frequency and : is the inner product of second order tensors. Using 1D assumptions for the length extensional mode of a piezoelectric rod, Eq. 3.2 simplifies to

$$P = \frac{1}{2}\omega \mathrm{Im}(E_3 D_3^* + T_3 S_3^*). \tag{3.3}$$

Thus with a suitable model for the electric and mechanical fields of the piezoelectric rod, the power dissipation density in the material can be calculated as a function of frequency and space.

3.2 Previous work on power dissipation in piezoelectric materials

There are multiple methods for modelling the power dissipation in piezoelectric materials. It is common to assume that the power dissipation in a piezoelectric material is spatially independent. An example of this is shown in Uchino and Hirose's study on loss mechanisms in piezoelectric materials [25]. In this work, the total power dissipation as a result of the mechanical, dielectric and piezoelectric losses is calculated. The power dissipation is then assumed to be uniform in the piezoelectric slab. When modelling the power dissipation in a transducer, the power dissipation density can be assumed to be uniform over the piezoelectric material to simplify the model [13].

A more detailed model of the power dissipation density in piezoelectric materials can take into account the spatial dependency throughout the material. Thomas et

al. modelled the power dissipation density across a piezoelectric slab in the d_{31} mode. In this case, it was found that the power dissipation as a result of the mechanical and piezoelectric loss were negligible for a piezoelectric slab under electrical excitation at a low frequency [42].

3.3 The power dissipation density and its contributions in a piezoelectric rod

3.3.1 Theory

Combining Eqs. 2.3 and 3.3 gives the following equation for the power dissipation density in a piezoelectric rod:

$$P = \frac{1}{2}\omega \mathrm{Im}(E_3 d_{33}^* T_3^* + E_3 \varepsilon_{33}^{T*} E_3^* + T_3 s_{33}^{E*} T_3^* + E_3^* d_{33}^* T_3). \tag{3.4}$$

Based on Eq. 3.4, there are four terms that contribute to the power dissipation density in a piezoelectric rod. The power dissipation density can be separated into three contributions as

$$P = P_{d,1} + P_{d,2} + P_{d,3}, \tag{3.5}$$

where

$$\begin{aligned} P_{d,1} &= \frac{1}{2}\omega \mathrm{Im}(T_3 s_{33}^{E*} T_3^*), \\ P_{d,2} &= \frac{1}{2}\omega \mathrm{Im}(E_3 \varepsilon_{33}^{T*} E_3^*), \\ P_{d,3} &= \frac{1}{2}\omega \mathrm{Im}(E_3 d_{33}^* T_3^* + E_3^* d_{33}^* T_3). \end{aligned}$$

The term $P_{d,1}$, which is associated with mechanical constants, can be interpreted as the mechanical contribution to the total power dissipation density [24, 42]. The same reasoning can be applied to $P_{d,2}$ which can be interpreted as the electrical contribution and $P_{d,3}$ could be interpreted as the piezoelectric contribution. The separation of the power dissipation density into these contributions inherently associates these mechanical, dielectric and piezoelectric losses with a particular physical mechanism. At first glance, Eq. 3.5 would appear to fulfill the goal of quantifying the importance of the mechanical, electrical and piezoelectric contributions to the

power dissipation density. This would then determine whether the piezoelectric contribution can truly be considered negligible. An equally valid method of quantifying the contributions to power dissipation density in a piezoelectric rod would be to use the g-form of the constitutive piezoelectric equations. Indeed, combining the g-form of the piezoelectric constitutive equation (Eq. 2.2 and Eq. 3.3) gives the following equation for the power dissipation density in a piezoelectric rod

$$P = \frac{1}{2}\omega \mathrm{Im}(T_3 s_{33}^{D*} T_3^* + D_3 \beta_{33}^T D_3^* - T_3 g_{33}^E D_3^* + T_3 g_{33}^* D_3^*). \tag{3.6}$$

This can also be separated into three contributions as

$$P = P_{g,1} + P_{g,2} + P_{g,3}, \tag{3.7}$$

where

$$\begin{aligned} P_{g,1} &= \frac{1}{2}\omega \mathrm{Im}(T_3 s_{33}^{D*} T_3^*), \\ P_{g,2} &= \frac{1}{2}\omega \mathrm{Im}(D_3 \beta_{33}^T D_3^*), \\ P_{g,3} &= \frac{1}{2}\omega \mathrm{Im}(-T_3 g_{33} D_3^* + T_3 g_{33}^* D_3^*). \end{aligned}$$

In a similar manner to the d-form, $P_{g,1}$ is interpreted as the mechanical contribution, $P_{g,2}$ the electrical contribution and $P_{g,3}$ the piezoelectric contribution. The difference between the contributions as a result of the d-, e-, h- and g-form piezoelectric constitutive equations will be investigated in the results.

The total power dissipation in the piezoelectric rod and its contributions as a function of frequency is also investigated in the results. The total power dissipation Ω in the piezoelectric rod and its contributing terms are given by

$$\Omega = A \int_0^L P \mathrm{d}x_3 = \Omega_{s,1} + \Omega_{s,3} + \Omega_{s,3}, \tag{3.8}$$

where A is the cross sectional area of the piezoelectric rod, L is the length of the piezoelectric rod, s is the piezoelectric constitutive form used and

$$\Omega_{s,n} = A \int_0^L P_{s,n} \mathrm{d}x_3 \tag{3.9}$$

where $n = 1, 2, 3$. It follows that $\Omega_{s,1}$, $\Omega_{s,2}$ and $\Omega_{s,3}$ are interpreted as the mechanical, electrical and piezoelectric contribution to the total power dissipation in the piezoelectric rod. It is important to note that although there is a requirement for

Table 3.1: List of the material parameters for the piezoelectric rod used in this study.

Material Constants	Value
s_{33}^D $[10^{-12} \times \mathrm{m}^2/\mathrm{N}]$	$7.80 - 0.31j$
β_{33}^T $[10^8 \times \mathrm{m/F}]$	$1.16 + 0.0033j$
g_{33} $[10^{-2} \times \mathrm{Vm/N}]$	$2.34 - 0.02j$
ρ $[\mathrm{kg/m}^3]$	7500

the total power dissipation density to be positive, this requirement does not apply to the individual contributions. Indeed, $\Omega_{s,3}$ has been shown to be negative in previous studies [43].

3.3.2 Method

Through the use of the 1D Mason model, Fig. 2.4, and Eq. 3.5, the contributions for the different piezoelectric constitutive forms are calculated for a piezoelectric rod with dimensions 3mm × 3mm × 20mm made of EDO EC-69 as a function of frequency and spatial position. The material parameters for EDO EC-69 are shown in Tab. 3.1. The piezoelectric material parameters originate from a full characterisation of EDO EC-69 with anisotropic losses [7].

3.3.3 Results

The frequency and spatially dependent power dissipation density and its contributing terms for the d-form in the piezoelectric rod are shown in Fig. 3.1. It is clear that the mechanical contribution is the most dominant of the three contributions. However, the results also show that the piezoelectric contribution is negative over certain parts of the frequency spectrum. It is therefore difficult to reconcile the negative contribution for the piezoelectric constant with a physical mechanism.

The comparison between the spatially dependent contributions for the different piezoelectric constitutive forms is shown in Fig. 3.2 at the resonance frequency. It can

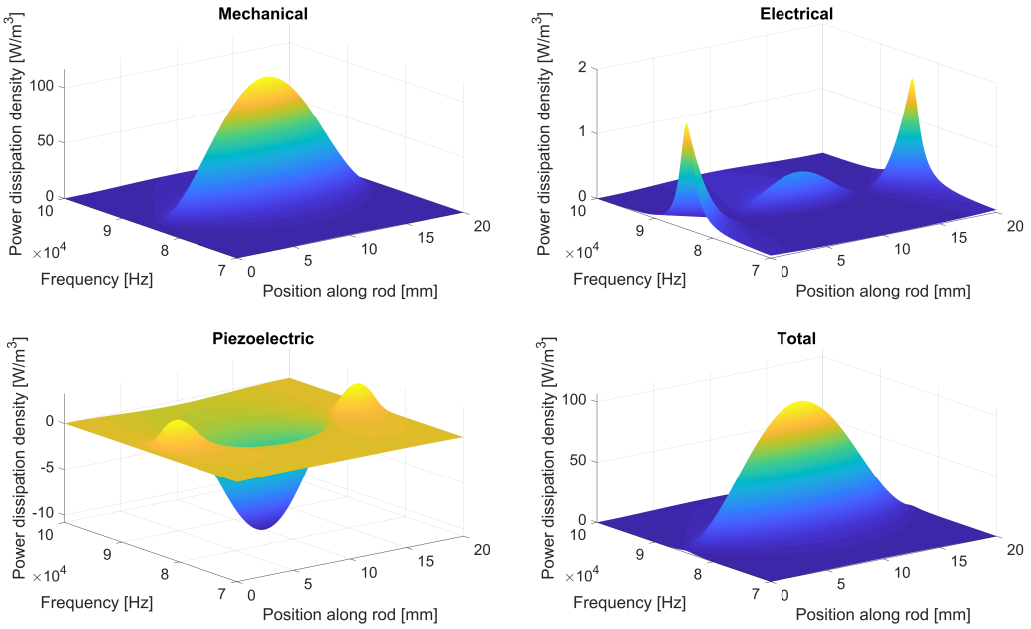

Figure 3.1: Power dissipation density as a function of frequency and position along the length of the rod for the mechanical contribution $P_{d,1}$, the electrical contribution $P_{d,2}$, the piezoelectric contribution $P_{d,3}$ and the total power dissipation density P.

be seen that there is no unique mechanical, electrical and piezoelectric contribution if the contributions are defined in the same manner described in Eq. 3.5. Furthermore, separating the contributions in this manner results in a mechanical contribution larger than the total power dissipation density and a negative contribution from the piezoelectric constants. The dielectric contribution remains largely negligible for all forms.

The total power dissipation and its three contributions are shown for each form in Fig. 3.3. These results confirm the conclusions from Fig. 3.2 that the contributions are different for different forms over the frequency range. Additionally, Fig. 3.3 also shows that for some of the piezoelectric constitutive forms, the power dissipation at frequencies near the resonance frequency are not completely dominated by the power dissipation as a result of the mechanical constants as is usually assumed. Indeed, for the g- and h-form, the contribution from the piezoelectric constants is not negligible at the resonance frequency. There are other parts of the spectrum where the contribution from the mechanical constants is overtaken by other contributions. In the e-form, the piezoelectric and electrical contribution dominate at frequencies

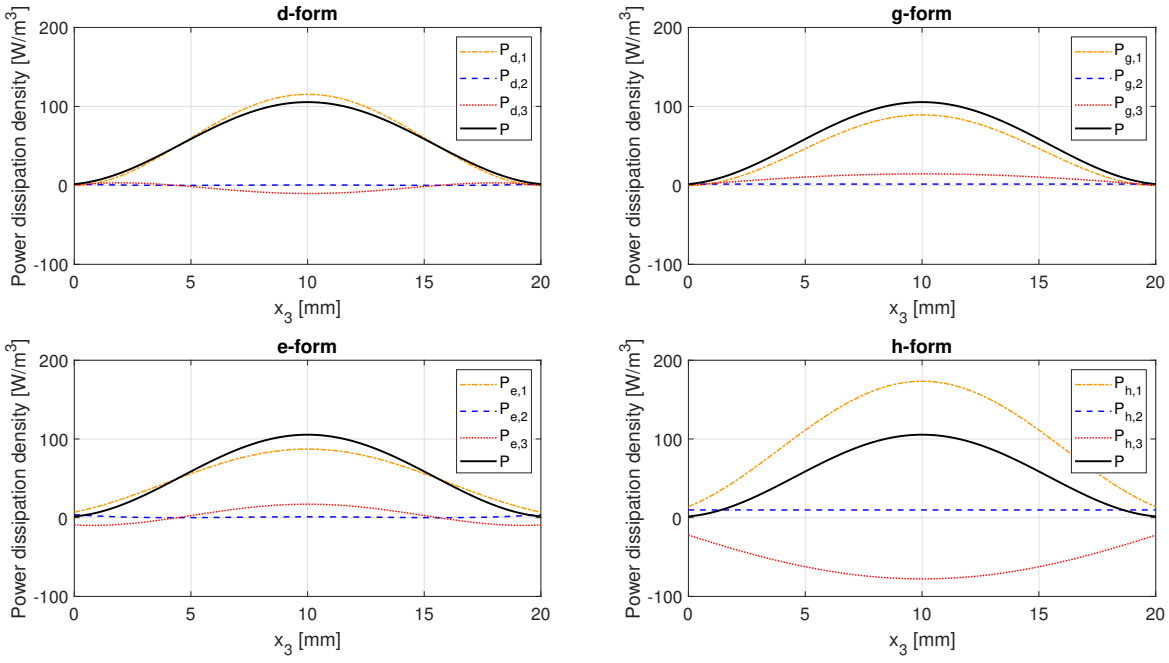

Figure 3.2: Power dissipation density as a function of position along the length of the rod. $P_{s,1}$ is interpreted as the mechanical contribution, $P_{s,2}$ is interpreted as the electrical contribution and $P_{s,3}$ is interpreted as the piezoelectric contribution where s is the piezoelectric constitutive equation form used. P is the total power dissipation density due to all the contributions.

larger than the antiresonance frequency.

This study initially demonstrated that there is no unique mechanical, electrical or piezoelectric contribution. It is therefore not recommended to attach any physical meaning to the losses, from which the power dissipation expressions are derived from. This is commonly seen in the literature when the piezoelectric loss is considered negligible as the loss due to piezoelectric energy conversion is low. It is also common to assume that the power dissipation at the resonance frequency is mainly due to the mechanical constants, whereas this is not necessarily the case as is shown in the h- and g-form. In this particular case for EDO-EC 69, the contribution from the dielectric constants is the smallest.

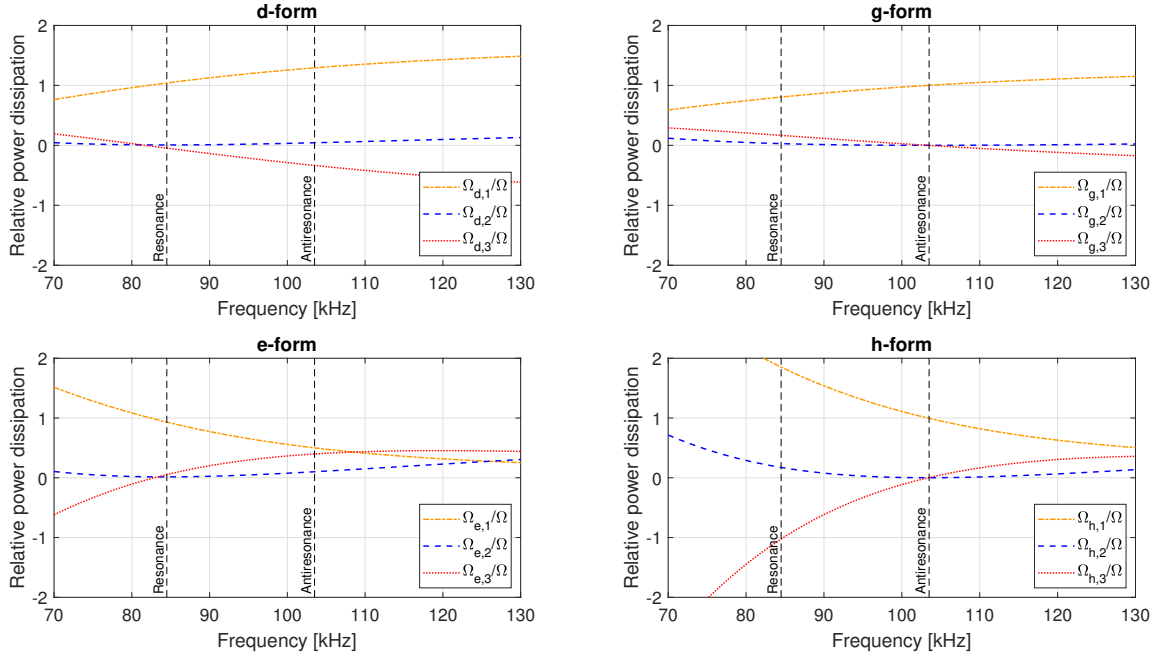

Figure 3.3: Power dissipation contributions relative to the total power dissipation as a function of frequency along the length of the rod. $\Omega_{s,1}$ is interpreted as the mechanical contribution, $\Omega_{s,2}$ is interpreted as the electrical contribution and $\Omega_{s,3}$ is interpreted as the piezoelectric contribution where s is the piezoelectric constitutive equation form used. Ω is the total power dissipation density due to all the contributions.

3.4 The comparison of the power dissipation in a transducer as a result of two representations of loss

There are two common representations of losses in piezoelectric materials which were discussed in section 2.3. The first is the IEEE Standard on Piezoelectricity which has two loss mechanisms, the mechanical quality and the dielectric loss. The second representation is the one predominantly used in this thesis, Holland's representation, which has three loss mechanisms at work. It is usual to only have the losses from the IEEE Standard representation supplied by the piezoelectric manufacturer. It is also common that these supplied losses are then used in distributed models as the imaginary part of the material constants [29]. As the piezoelectric loss is not

supplied, the piezoelectric constant is considered real. This study aimed to quantify the consequence of using the losses as a result of the IEEE Standard method as complex parameters in a distributed model in the way losses are defined under Holland's representation [22].

3.4.1 Method

The impedance of a piezoelectric plate made of PZ27 with a thickness of 7.5mm and a diameter of 15cm is modelled using the 1D Mason model (Fig. 2.4) and the material parameters characterised using Holland's representation [44]. The impedance is then used to characterise the material parameters using the IEEE Standard method which uses the BVD model. Under Holland's notation, there are six parameters, with three loss mechanisms defined as the imaginary part of the material constants. Under the IEEE Standard method, there are five parameters: three material constants, the mechanical quality and the dielectric loss. The material parameters as a result of the two characterisation methods are shown in Tab. 3.2 implemented using Holland's representation. The aim of the study is to determine whether the power dissipation calculated as a result of these two material data sets, both implemented as complex material constants, is different. To further demonstrate this, the power dissipation is modelled for a complete plate transducer model to determine whether the discrepancy between the two material data sets has any effect on the calculated power dissipation in a transducer model. The temperature rise as a result of the two power dissipation calculations is modelled and compared to quantify the effect the difference between the two characterised material parameter sets has on a temperature model. The plate transducer schematic and surrounding thermal conditions is shown in Fig. 3.4, with GRP as the matching layer and Silicone rubber used for the backing layer. The thermal, mechanical and piezoelectric material parameters for all materials are shown in Tab. 3.2.

3.4.2 Results

The comparison of the distribution of the power dissipation density throughout the transducer stack as a result of the two material data sets is shown in Fig. 3.5.

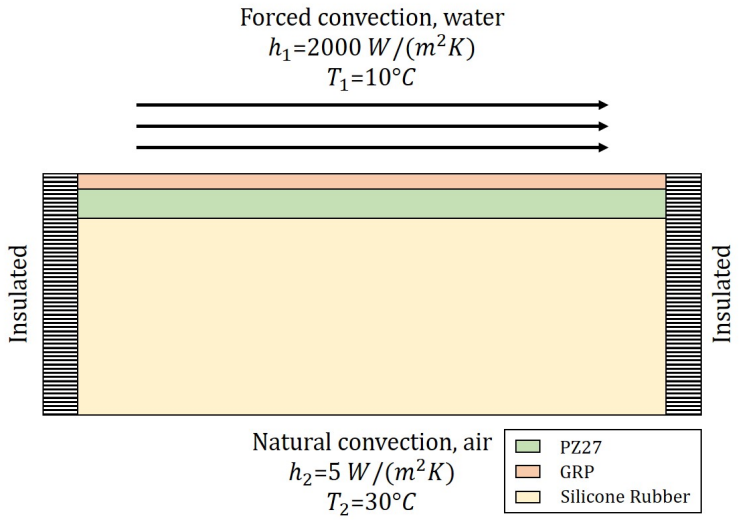

Figure 3.4: Transducer schematic slice with thermal boundary conditions. h is the convection coefficient.

Table 3.2: List of the material parameters for the materials used in the transducer. There are two material data sets for PZ27 based on the two representations in piezoelectric materials.

Material Constants			Silicone Rubber	GRP	PZ27	
					Holland [24]	IEEE Std. [18]
Elastic Modulus	E	GPa	0.014	16.4		
Poisson Ratio	ν		0.48	0.44		
Mechanical Quality	Q_m		50	100		
Mechanical stiffness	c_{33}^D	GPa			$129 + 0.21j$	$129 + 0.28j$
Electric impermittivity	ε_{33}^S	$10^8 \times$ m/F			$1.49 + 0.021j$	$1.53 + 0.022j$
Piezoelectric constant	h_{33}	$10^9 \times$ V/m			$2.10 + 0.013j$	2.24
Density	ρ	kg/m^3	1150	2020	7500	
Thermal conductivity	k	W/mK	0.14	0.04	1.8	
Specific heat capacity	C_p	J/kgK	1175	700	420	
Layer thickness		mm	50	3.75	7.5	

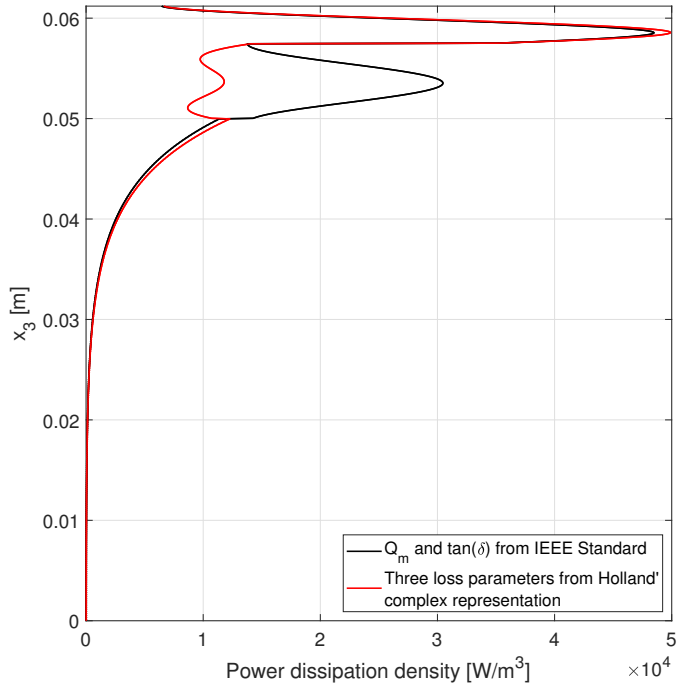

Figure 3.5: Comparison of the power dissipation density as a result of the two representations of loss throughout the transducer at the resonance frequency, 250kHz.

There is a clear discrepancy between the power dissipation density distribution at the piezoelectric layer. Indeed, the power dissipation density is much larger using the IEEE Standard material parameters than it is for the parameters characterised using Holland's representation. Although the discrepancies aren't as significant, there is still a difference between the two models in the backing and matching layer. Therefore, the discrepancy in the material parameters in the piezoelectric material propagates to the surrounding materials.

Fig. 3.6 shows the resulting steady state temperature throughout the transducer for the boundary conditions in Fig. 3.4 and power dissipation density distributions in Fig. 3.5. There is a difference of up to 7°C in the predicted steady state temperature between the two power dissipation density models. The difference in steady state temperature between the two models is spread out over the length of the transducer.

These results demonstrate that the loss parameters determined using the IEEE Standard on Piezoelectricity, the mechanical quality and dielectric loss, are not equivalent to the loss parameters determined using Holland's representation. It is

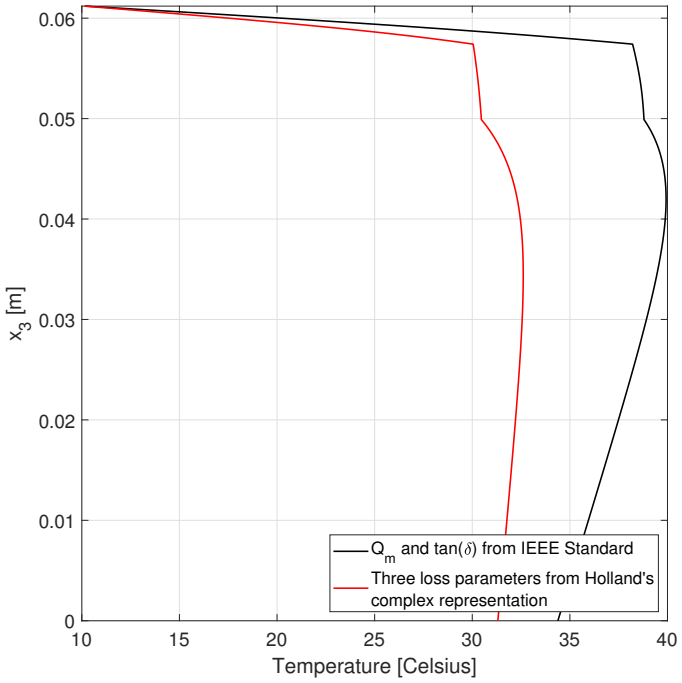

Figure 3.6: Comparison of the steady state temperature as a result of the two representations of loss throughout the transducer at the resonance frequency, 250kHz.

therefore not recommended to use the mechanical quality and dielectric loss parameters supplied by the manufacturer as the imaginary component of the mechanical and dielectric constants for distributed models.

Chapter 4

Temperature distribution in a piezoelectric rod

A characterisation method was developed in order to determine the loss parameters of a piezoelectric rod. The goal of this chapter is to validate the material parameters determined by the characterisation method. In order to validate the characterisation method, the spatially dependent temperature profile in the piezoelectric rod as a result of the predicted power dissipation density profile is compared to the measured temperature profile in the piezoelectric rod. If the validation is successful, this would demonstrate that once the piezoelectric material parameters are determined using the characterisation method, then the temperature rise can be predicted for a given frequency and voltage. These material parameters could then confidently be used in a temperature model of the transducer in the design phase. This chapter starts by reviewing previous work on the prediction or measurement of the temperature rise in piezoelectric materials. The results of the comparison between the predicted and measured spatially dependent temperature rise in the piezoelectric rod are then presented.

4.1 Previous studies on thermal modelling in piezoelectric materials

It is common to treat the temperature distribution as constant in space for piezoelectric materials [45, 46, 32, 47]. The temperature in the piezoelectric material can be measured using a thermocouple that is thermally coupled to the sample using thermal grease or paste. Another measurement technique uses an infrared spot thermometer, which has the advantage of being a non-contact method and therefore does not affect the vibration pattern of the sample. These methods measure the temperature in a single spot on the sample and the temperature throughout the sample is considered to be equal to the temperature at that spot. These are robust methods that yield good results when compared with a predicted temperature model that is spatially uniform.

A number of studies have measured and predicted the spatially distributed temperature rise throughout a piezoelectric sample. Joo et al. predicted and measured the spatial distribution of the temperature rise throughout a piezoelectric transformer [48]. The temperature distribution was measured using an infrared camera and modelled using FEM. The shape of the steady state temperature rise along the lateral length of the transformer was captured very well. However, the absolute temperature rise was underestimated. The study also demonstrated the importance of modelling the temperature rise with temperature dependent material constants if the temperature increase is significant. Thomas et al. modelled the spatial distribution of the power dissipation density in a piezoelectric slab in a similar manner to the method used in this project [42]. Based on this spatially distributed power dissipation density, the temperature in a piezoelectric slab is predicted for various thermal conditions. These are compared to the predicted temperature given a spatially constant power dissipation density in the piezoelectric slab. The study shows that the temperature rise difference between the centre and the edge of the slab is more accentuated for the spatially distributed model than it is for the spatially constant power dissipation density model. Hu et al. modelled and measured the spatial distribution of temperature for a piezoelectric bar used as a transformer [49, 50].

The temperature rise along the length of the piezoelectric material was measured using an infrared camera. There was good agreement between the modelled and measured steady state temperature rise.

4.2 Comparison between the measured and modelled spatially distributed temperature along the length of a piezoelectric rod.

The goal of this PhD was to predict the spatially distributed temperature rise along the length of a piezoelectric rod. This was achieved by modelling the temperature rise in a piezoelectric rod given a spatially distributed power dissipation density as calculated in Section 3.1 for a particular voltage and frequency from the characterised material parameters determined using the method shown in Section 2.5. The predicted temperature rise is compared to the measured spatial distribution of the temperature rise along the length of the rod. The first goal of this comparison is that this would determine whether the characterised material parameters from the characterisation method can be used to accurately predict the temperature rise in a piezoelectric material. The second goal is to determine whether Holland's representation, a very useful approximation for narrow frequency ranges, can be practically used to predict the spatial distribution of the power dissipation density accurately in a piezoelectric material given its inherent assumptions.

The first part of this paper concentrated on characterising the piezoelectric material, PZT5A1, at a voltage of 40 V. Indeed, to attain a meaningful temperature rise, a higher voltage was needed. Therefore the impedance of the piezoelectric rod needed to be measured with a driving voltage of 40 V to characterise the material parameters. However, impedance analysers are typically limited to small signal levels, only a couple of volts. Therefore, a different experimental setup was developed to calculate the impedance of the piezoelectric rod at higher voltages. The material parameters as a result of this characterisation were then used to predict the spatially distributed power dissipation density in the piezoelectric rod. This power dissipation density profile is used as the heat generation term in a thermal FEM model of

the piezoelectric rod. For comparison, a constant power dissipation density profile is also used as the heat generation term in the FEM model. This would show whether it makes a practical difference to use a spatially distributed power dissipation density as opposed to a spatially uniform power dissipation density distribution. Finally, the modelled temperature for both power dissipation density distributions are compared to the measured temperature distribution with the same thermal boundaries.

4.2.1 Characterising the nonlinearity in a piezoelectric rod

The material parameters of piezoelectric materials change with voltage amplitude. Indeed, the voltage was shown to have an effect on the resonance peak in the admittance spectrum by Uchino et al. [32]. In order to determine the material parameters for higher voltages, the characterisation method from Section 2.5 was implemented using an impedance curve measured at higher voltages. A different experimental method, shown in Fig. 4.1, to measure the impedance of the piezoelectric was developed. In this measurement setup, the voltage is measured over the piezoelectric rod and sense resistor in channel 1 of the oscilloscope. The current through the piezoelectric material is derived from the voltage over channel 2, which measures the voltage over the sense resistor. The signal generator sweeps the frequency range of interest and the power amplifier amplifies the signal to the desired voltage of interest. An issue with measuring the impedance in this manner is that the piezoelectric material can heat up during the measurement. As the temperature can also have an effect on the material properties, the measurement setup had to be modified to avoid heating the piezoelectric material up as the impedance was being measured. Therefore, a thermocouple was placed on the sample to ensure that the piezoelectric material cooled below a minimum threshold temperature before the next frequency sample was taken.

Using the experimental setup, the voltage dependency of the admittance was measured and is shown in Fig. 4.2. It can be seen that even for low voltage increases, there is a significant effect on the resonance peak in the admittance spectrum. The resonance frequency is shifted towards the lower frequencies and the peak is damped as the voltage increases. The effect on the antiresonance peak is not very significant.

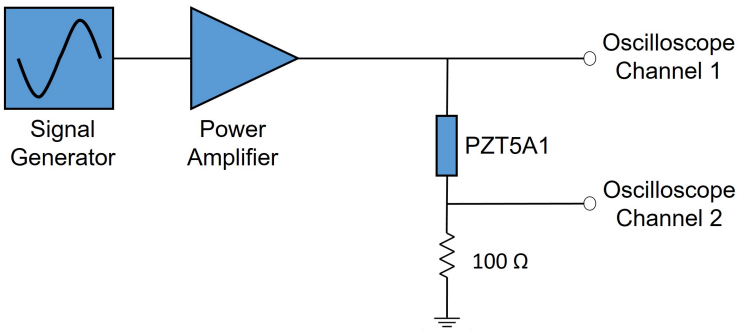

Figure 4.1: Electrical setup to measure the impedance at higher voltages. Channel 1 of the oscilloscope measures the voltage whilst Channel 2 is used to derive the current over PZT5A1

Table 4.1: List of the material parameters for the piezoelectric rod used in this study compared with the material parameters determined at low driving voltage using an impedance analyser.

Material parameters		Small signal	40 V
Symbol	Dimensions	values	values
s_{33}^D	$10^{-12} \times \mathrm{m}^2/\mathrm{N}$	$6.68 + 0.009j$	$11.0 - 0.02j$
β_{33}^T	$10^7 \times \mathrm{m/F}$	$6.27 + 0.1j$	$6.75 + 0.28j$
g_{33}	$10^{-2} \times \mathrm{Vm/N}$	$2.57 - 0.01j$	$2.27 - 0.02j$
ρ	$\mathrm{kg/m}^3$	7750	7750

This is similar to the findings by Uchino et al. but for a smaller range of voltage amplitudes. This has a significant effect on the characterised material parameters. These are shown in Tab. 4.1. The effect seems to affect the mechanical constants the most.

4.2.2 Power dissipation density model

To predict the temperature rise in the piezoelectric rod, the spatial distribution of the power dissipation density was modelled. The power dissipation density spatial distribution along the length of the rod can be modelled using the equations in Section 3.1. Given the material parameters characterised at 40 V in Tab. 4.1, the spatial distribution of the power dissipation density is shown in Fig. 4.3 at 68 kHz.

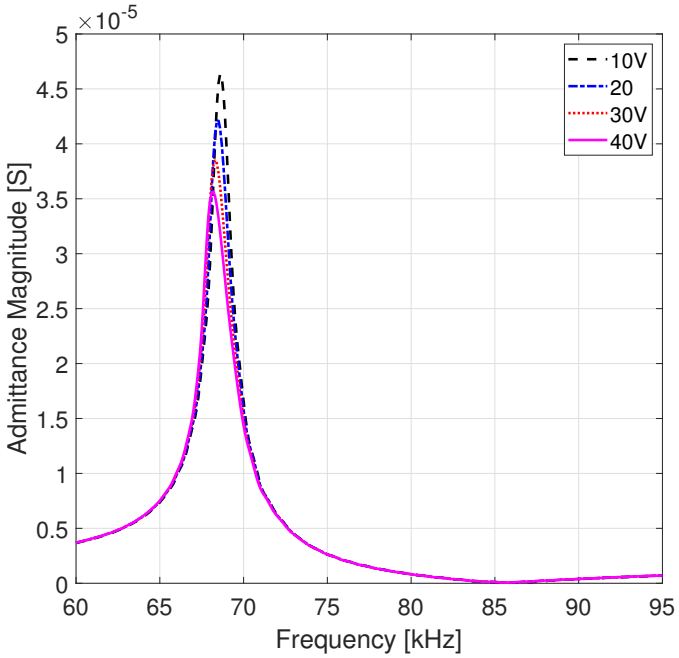

Figure 4.2: The admittance of the piezoelectric rod PZT5A1 as a function of voltage amplitude. As the voltage increases, the resonance frequency reduces and the resonance peak is damped.

The power dissipation density is predicted to be more than two times larger in the centre of the rod than at the edges of the rod. The second power dissipation density curve in Fig. 4.3 is constant in space. To simplify the thermal model, the power dissipation density can be assumed to be constant in space for ultrasound transducers where the piezoelectric layer is only one of the components. Modelling the temperature rise in the piezoelectric rod with the constant power dissipation curve will show whether using a spatial distribution of power dissipation density makes any practical difference or whether a constant power dissipation density is adequate enough.

4.2.3 Temperature model and measurement

The spatial distribution of the temperature along the length of the piezoelectric rod is measured using an experimental setup shown in Fig. 4.4. In this setup, the piezoelectric rod is placed in a container made of Ebazell 160, a thermally insulating material. In this manner, the air inside the container can be assumed to be independent of the air outside the box, thus rendering the convection rate

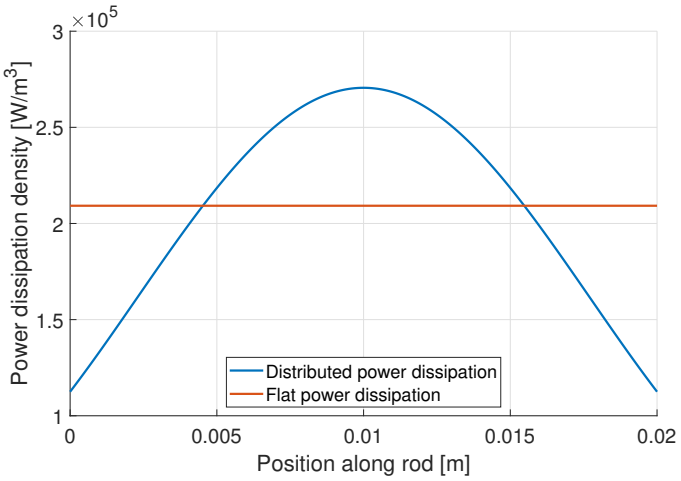

Figure 4.3: Two modelled spatial distributions of the power dissipation density along the length of piezoelectric rod.

more stable. There are five thermocouples in total in the setup. Three of those thermocouples are placed on the surface of the piezoelectric rod and measure the temperature at the edge (TC 1), a quarter way along the length (TC 2) and at the centre (TC 3) of the piezoelectric rod as shown in Fig. 4.4. The temperature is only measured on one half of the rod as it is assumed to be symmetric with respect to the centre of the rod. The fourth thermocouple (TC 4) measures the air temperature inside the container. The final thermocouple (TC 5) measures the temperature where the copper wire exits the container. The piezoelectric material is excited through the copper wires using a signal generator and power amplifier to achieve a peak voltage of 40 V. The piezoelectric material is excited for 10 minutes and then allowed to cool down before the next measurement is taken. The measurement was repeated five times in order to quantify the uncertainty of the measurement.

A FEM model of the temperature measurement was then built and simulated in COMSOL. The model is shown in Fig. 4.5 and carries a few assumptions in order to reduce the computation time of the model. As the temperature is assumed to be symmetrical with respect to the centre of the rod, only half of the rod is simulated and there is a symmetry boundary condition. As the container is small, the air temperature is assumed to be constant in space and equal to the temperature measured by TC 4. The boundary of the model is where the copper wire exits the container, where the temperature is set equal to the temperature measured by TC 5.

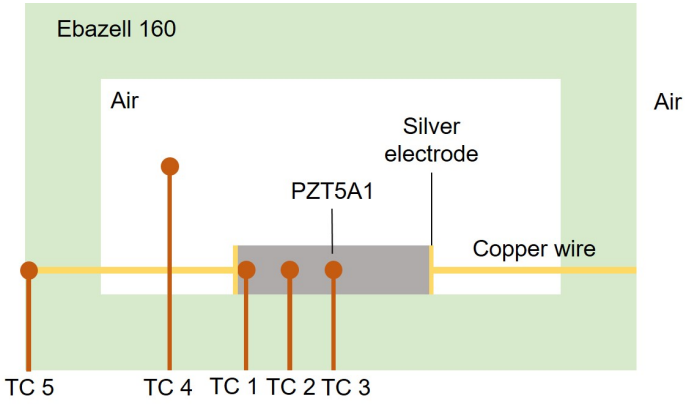

Figure 4.4: Schematic of the temperature measurement showing the placement of the thermocouples. TC stands for thermocouple. TC 1, 2 and 3 measure the temperature along the length of the piezoelectric rod. TC 4 measures the air temperature in the container and TC 5 measures the temperature where the copper wire exits the container.

Table 4.2: List of the thermal material parameters used in the temperature model. The piezoelectric thermal material parameters originate from [51].

Materials parameters		PZT5A1	Silver	Copper
Name	Dimensions		electrodes	wire
Thermal conductivity	W/(mK)	1.2	429	400
Heat Capacity	J/(kgK)	320	235	385
Density	kg/m^3	7750	10500	8940
Emissivity	N/A	0.5	0	0

There is convection into the air along the copper wire, electrode and piezoelectric material. There is also radiation at the surface of the piezoelectric material. Finally, the power dissipation density curves in Fig. 4.3 are used as the heat source in the model. The thermal properties of the materials in the model are shown in Tab. 4.2.

4.2.4 Results

Figs. 4.6 and 4.7 show the results of the models and measurements as a function of time for TC 1, 2 and 3 for both power dissipation density curves in Fig. 4.3. The measured data shows a clear trend, even with uncertainties taken into account,

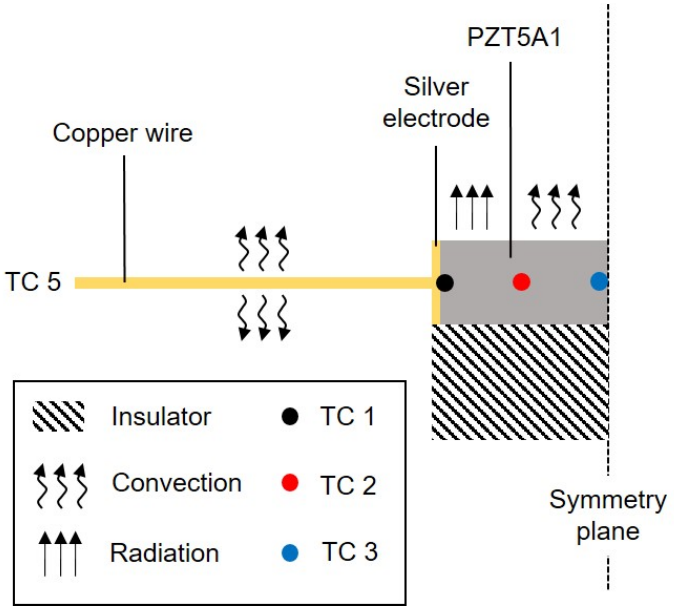

Figure 4.5: Schematic of the model in COMSOL with the boundary conditions shown. The model shows half of the experimental setup as the temperature is considered symmetric with respect to the centre of the rod. There is convection into air at the copper wire, electrodes and piezoelectric material. There is also radiation from the piezoelectric material into the surrounding area. The piezoelectric rod is resting on the Ebazell material which is considered to be a perfect insulator in the model.

where the temperature at TC 1 increases the least whilst the temperature at TC 3 increases the most of the three thermocouples. The temperature at TC 2 is evenly space between the temperatures measured at TC 1 and TC 3.

Based on the spatially distributed power dissipation curve, where the power dissipation density is larger at the centre of the rod than at the edges, the modelled data should show the same trend as the one shown in the measured data. The modelled data in Fig. 4.6 does have the same trend, with the temperature at TC 1 increasing the least and the temperature at TC 3 increasing the most. However, the modelled temperature curve does not track the measured temperature curve completely. Indeed, the model initially underestimates the heating rate up until approximately 200 seconds. After 200 seconds, the model overestimates the heating rate and at 600 seconds, the final time sample, the model has overestimated the temperature rise.

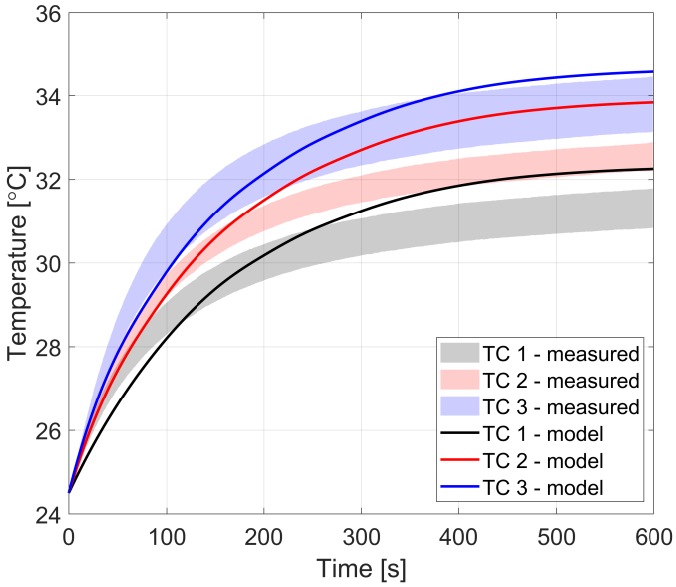

Figure 4.6: Measured and modelled temporal temperature dependence of TC 1, 2 and 3 for a spatially distributed power dissipation density. Note that the measured data covers a range of temperatures for each time sample to show the uncertainty associated with the measurement.

Fig. 4.7 shows the modelled temperature curves at TC 1, 2 and 3 for a power dissipation density that is constant in space compared with the measured data. The modelled temperature at TC 1 increases the least whilst the modelled temperature at TC 3 increases the most. This trend is the same as the the one in the measured data and the modelled temperature as a result of the spatially distributed power dissipation density. It also does not track the measured data completely in a similar manner to the modelled data in Fig. 4.6. However, the difference between the modelled temperature at TC 1 and TC 3 at 600 seconds is clearly smaller in Fig. 4.7 than it is in Fig. 4.6. The difference at 600 seconds between TC 1 and TC 3 is 8% for the mean value of the measured data, 7% for the spatially distributed power dissipation density model and 4.3% for the spatially constant power dissipation density model. This would suggest that the model with the spatially distributed power dissipation density captures the behaviour of the piezoelectric material better than the model with the spatially constant power dissipation density. This further appears to confirm that Holland's representation of losses in piezoelectric materials, in coordination with the generalised Poynting vector, is adequate for modelling the

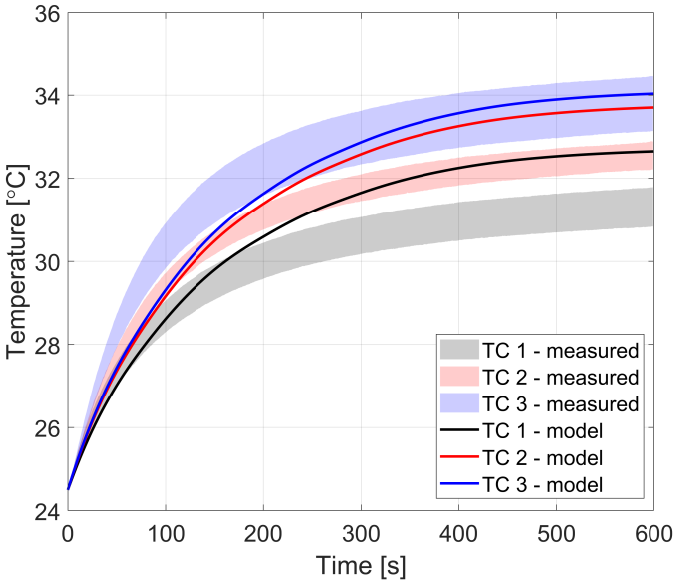

Figure 4.7: Measured and modelled temporal temperature dependence of TC 1, 2 and 3 for a power dissipation density that is constant in space. Note that the measured data covers a range of temperatures for each time sample to show the uncertainty associated with the measurement.

spatial distribution of the temperature in a piezoelectric rod.

4.2.5 Conclusion

The work in this section aimed to determine whether Holland's representation with characterised material parameters could adequately predict the spatial distribution of the power dissipation density in a piezoelectric rod. The previous two stages of the PhD thesis characterised the material constants and power dissipation density using Holland's representation based on a measured impedance curve. It was therefore important to verify the two previous stages of the PhD. This verification takes the form of Fig. 4.6 which compares the predicted and measured temperature distribution.

It was determined that the physical shape of the spatial distribution of the power dissipation density along the length of the piezoelectric rod is more similar to the spatially distributed curve in Fig. 4.3 than it is to a power dissipation density which is constant in space. This was the conclusion based on the difference in temperature between TC 1 and 3 at the final time of 600 seconds. This, therefore, bolsters

the suggestion that given a well executed characterisation of the piezoelectric material, the temperature can be adequately predicted. This is an important finding for transducer designers as once the piezoelectric material is characterised, the temperature increase for a given excitation in a transducer stack can confidently be predicted. Thus, the transducer design can be tweaked in order to reduce the temperature increase, especially at important points. In order to increase the accuracy of the prediction, it is also clear that more accurate thermal material parameters are needed.

Chapter 5

Conclusion

This thesis outlined the development of a characterisation method followed by the prediction and verification of the power dissipation density and temperature profile along the length of a piezoelectric rod as a result of the determined material parameters.

The piezoelectric loss was demonstrated to be a unique parameter in Holland's representation of loss. The use of two cost functions, one based on the impedance and the other based on the admittance, was shown to mitigate the effect of noise on the characterised material parameters. Another finding in the development of the characterisation method was that using a local optimisation with the manufacturer data could lead to the characterisation method finding a local minimum instead of the global minimum.

The importance of each loss mechanisms' contribution to the power dissipation in the piezoelectric material was quantified. Although the power dissipation can be separated into a contribution that originates from the mechanical, electrical and piezoelectric constants, this separation is arbitrary. Indeed, the contributions from the mechanical, electrical and piezoelectric losses changed depending on the piezoelectric constitutive equation used. Furthermore, the piezoelectric contribution was negative over parts of the frequency spectrum. Therefore, it was concluded that it is not recommended to attach the loss parameters to specific physical mechanisms.

Finally, the temperature rise in the piezoelectric rod was predicted using the characterised material parameters determined in the first stage of the PhD. This

was compared to the measured temperature rise in the piezoelectric rod. It was determined that although the thermal material parameters needed to be characterised better, the temperature difference between the edge and centre of the rod compared well between the measured and modelled data.

Bibliography

[1] J. L. Butler and C. H. Sherman, *Transducers and Arrays for Underwater Sound*, 2nd ed. Springer, New York, 2016, ch. 3, pp. 123–124.

[2] N. P. Sherlock and R. J. Meyer, "Modified single crystals for high-power underwater projectors," *IEEE Trans. Ultrason., Ferroelect., Freq. Control*, vol. 59, no. 6, pp. 1285–1291, Jun. 2012.

[3] H. J. Lee, S. Zhang, Y. Bar-Cohen, and S. Sherrit, "High temperature, high power piezoelectric composite transducers," *Sensors*, vol. 14, no. 8, pp. 14 526–14 552, Aug. 2014.

[4] A. C. S. Parr, R. L. O'Leary, and G. Hayward, "Improving the thermal stability of 1-3 piezoelectric composite transducers," *IEEE Trans. Ultrason., Ferroelect., Freq. Control*, vol. 52, no. 4, pp. 550–563, Apr. 2005.

[5] C. Richard, H. Lee, and D. Guyomar, "Thermo-mechanical stress effect on 1–3 piezocomposite power transducer performance," *Ultrasonics*, vol. 42, no. 1-9, pp. 417–424, Apr. 2004.

[6] P. N. Bilgunde and L. J. Bond, "Effect of thermal degradation on high temperature ultrasonic transducer performance in small modular reactors," *Physics Procedia*, vol. 70, pp. 433–436, 2015.

[7] R. G. Sabat, B. K. Mukherjee, W. Ren, and G. Yang, "Temperature dependence of the complete material coefficients matrix of soft and hard doped piezoelectric lead zirconate titanate ceramics," *J. Appl. Phys.*, vol. 101, p. 064111, Mar. 2007.

[8] S. Sherrit, G. Yang, H. Wiederick, and B. Mukherjee, "Temperature dependence of the dielectric, elastic and piezoelectric material constants of lead zirconate

titanate ceramics," in *Proceedings of the International Conference on Smart Materials, Structures and Systems*, Bangalore, India, Jul. 1999, pp. 121–126.

[9] J. Pastor, C. Richard, and H. Nguyen Viet, "Predicting the losses and the efficiency of a 1-3 piezo-composite transducer through a partial homogeneization method," *Boletín de la Sociedad Española de Cerámica y Vidrio*, vol. 41, no. 1, pp. 171–176, Feb. 2002.

[10] N. Abboud, J. Mould, G. Wojcik, D. Vaughan, D. Powell, V. Murray, and C. MacLean, "Thermal generation, diffusion and dissipation in 1-3 piezocomposite sonar transducers: Finite element analysis and experimental measurements," in *Proc. IEEE Ultrason. Symp.*, vol. 2. Toronto, Canada: IEEE, Oct. 1997, pp. 895–900.

[11] W.-S. Ohm, J. H. Kim, and E. C. Kim, "Prediction of surface temperature rise of ultrasonic diagnostic array transducers," *IEEE Trans. Ultrason., Ferroelect., Freq. Control*, vol. 55, no. 1, pp. 125–138, Jan. 2008.

[12] J. Calvert, F. Duck, S. Clift, and H. Azaime, "Surface heating by transvaginal transducers," *Ultrason. Obstet. Gynecol.*, vol. 29, no. 4, pp. 427–432, Apr. 2007.

[13] O. Saunders, S. Clift, and F. Duck, "Ultrasound transducer self heating: development of 3-D finite-element models," in *J. Phys.: Conf. Ser. 1*, no. 72, 2004, pp. 72–77.

[14] M. G. Curley, "Soft tissue temperature rise caused by scanned, diagnostic ultrasound," *IEEE Trans. Ultrason., Ferroelect., Freq. Control*, vol. 40, no. 1, pp. 59–66, Jan. 1993.

[15] H. J. Lee and S. Zhang, "Design of low-loss 1-3 piezoelectric composites for high-power transducer applications," *IEEE Trans. Ultrason., Ferroelect., Freq. Control*, vol. 59, no. 9, pp. 1969–1975, Sep. 2012.

[16] E. Hollenstein, D. Damjanovic, and N. Setter, "Temperature stability of the piezoelectric properties of Li-modified KNN ceramics," *J. Eur. Ceram. Soc.*, vol. 27, no. 13-15, pp. 4093–4097, Mar. 2007.

[17] S. Hirose, M. Aoyagi, Y. Tomikawa, S. Takahashi, and K. Uchino, "High power characteristics at antiresonance frequency of piezoelectric transducers," *Ultrasonics*, vol. 34, no. 2-5, pp. 213–217, Jun. 1996.

[18] "IEEE Standard on Piezoelectricity," *ANSI/IEEE Std 176-1987*, 1987.

[19] M. Wild, K. Hjelmervik, L. Hoff, and M. Bring, "Characterising piezoelectric material parameters through a 3D FEM and optimisation algorithm," in *OCEANS 2017-Aberdeen.* Aberdeen, UK: IEEE, Jun. 2017, pp. 1–5.

[20] M. Wild, M. Bring, L. Hoff, and K. Hjelmervik, "Characterization of piezoelectric material parameters through a global optimization algorithm," *IEEE J. of Ocean. Eng.*, pp. 1–9, Jan. 2019.

[21] M. Wild, M. Bring, E. Halvorsen, L. Hoff, and K. Hjelmervik, "The challenge of distinguishing mechanical, electrical and piezoelectric losses," *J. Acoust. Soc. Am.*, vol. 144, no. 4, pp. 2128–2134, Oct. 2018.

[22] M. Wild, M. Bring, L. Hoff, and K. Hjelmervik, "Comparison of two models for power dissipation and temperature in piezoelectric transducers," in *2018 IEEE International Ultrasonics Symposium (IUS).* Kobe, Japan: IEEE, Oct. 2018, pp. 1–4.

[23] G. Lie, S. Zhang, W. Jiang, and W. Cao, "Losses in ferroelectric materials," *Mater. Sci. and Eng. R*, vol. 89, pp. 1–48, Feb. 2015.

[24] R. Holland, "Representation of dielectric, elastic, and piezoelectric losses by complex coefficients," *IEEE Trans. Sonics Ultrason.*, vol. 14, no. 1, pp. 18–20, Jan. 1967.

[25] K. Uchino and S. Hirose, "Loss mechanisms in piezoelectrics: how to measure different losses separately," *IEEE Trans. Ultrason., Ferroelect., Freq. Control*, vol. 48, no. 1, pp. 307–321, Jan. 2001.

[26] D. J. Powell, J. Mould, and G. L. Wojcik, "Dielectric and mechanical absorption mechanisms for time and frequency domain transducer modeling," in *Proc.*

IEEE Ultrason. Symp., vol. 2. Sendai, Japan: IEEE, Oct. 1998, pp. 1019–1024.

[27] I. Mayergoyz and G. Bertotti, *The Science of Hysteresis, Volume 3*. Elsevier, 2005, ch. 4, pp. 367–368.

[28] L. P. Tran-Huu-Hue, F. Levassort, N. Felix, D. Damjanovic, W. Wolny, and M. Lethiecq, "Comparison of several methods to characterise the high frequency behaviour of piezoelectric ceramics for transducer applications," *Ultrasonics*, vol. 38, no. 1-8, pp. 219–223, Mar. 2000.

[29] M. Lethiecq, L. P. Tran-Huu-Hue, F. Patat, and L. Pourcelot, "Measurement of losses in five piezoelectric ceramics between 2 and 50 MHz," *IEEE Trans. Ultrason., Ferroelect., Freq. Control*, vol. 40, pp. 232–237, May 1993.

[30] S. Sherrit, S. P. Leary, B. P. Dolgin, and Y. Bar-Cohen, "Comparison of the Mason and KLM equivalent circuits for piezoelectric resonators in the thickness mode," in *Proc. IEEE Ultrason. Symp.*, vol. 2, Lake Tahoe, NV, USA, Oct. 1999, pp. 921–926.

[31] S. Sherrit and B. K. Mukherjee, "Characterisation of piezoelectric materials for transducers," *Dielectric and Ferroelectric Reviews.*, Nov. 2007.

[32] K. Uchino, Y. Zhuang, and S. O. Ural, "Loss determination methodology for a piezoelectric ceramic: new phenomenological theory and experimental proposals," *J. Adv. Dielectr.*, vol. 1, no. 1, pp. 17–31, 2011.

[33] K. W. Kwok, H. L. W. Chan, and C. L. Choy, "Evaluation of the material parameters of piezoelectric materials by various methods," *IEEE Trans. Ultrason., Ferroelect., Freq. Control*, vol. 44, no. 4, pp. 733–742, Jul. 1997.

[34] C. Y. Kiyono, N. Peréz, and E. C. N. Silva, "Determination of full piezoelectric complex parameters using gradient-based optimization algorithm," *Smart Mater. Struct.*, vol. 25, no. 025019, Jan. 2016.

[35] C. Joh, J. Kim, and Y. Roh, "Determination of the complex material constants of PMN–28%PT piezoelectric single crystals," *Smart Mater. Struct.*, vol. 22, no. 125027, Nov. 2013.

[36] S. J. Rupitsch and J. Ilg, "Complete characterization of piezoceramic materials by means of two block-shaped test samples," *IEEE Trans. Ultrason., Ferroelect., Freq. Control*, vol. 62, no. 7, pp. 1403–1413, Jul. 2015.

[37] T. Lahmer, M. Kaltenbacher, B. Kaltenbacher, R. Lerch, and E. Leder, "FEM-based determination of real and complex elastic, dielectric, and piezoelectric moduli in piezoceramic materials," *IEEE Trans. Ultrason., Ferroelect., Freq. Control*, vol. 55, no. 2, pp. 465–475, Feb. 2008.

[38] S. J. Rupitsch and R. Lerch, "Inverse method to estimate material parameters for piezoceramic disc actuators," *Appl. Phys. A*, vol. 97, no. 4, pp. 735–740, Oct. 2009.

[39] A. Mansoori, L. Hoff, and M. Wild, "A fem-based method for complete parameter identification of thin piezoceramic bars," in *2018 IEEE International Ultrasonics Symposium (IUS)*, Kobe, Japan, Oct., pp. 1–4.

[40] Z. Ugray, L. Lasdon, J. Plummer, F. Glover, J. Kelly, and R. Martí, "Scatter search and local NLP solvers: A multistart framework for global optimization," *INFORMS J. Comput.*, vol. 19, no. 3, pp. 328–340, Jul. 2007.

[41] B. A. Auld, *Acoustic fields and waves in solids*, 2nd ed. Wiley, New York, 1973, vol. 1, ch. 8, p. 311.

[42] D. Thomas, D. D. Ebenezer, and S. M. Srinivasan, "Power dissipation and temperature distribution in piezoelectric ceramic slabs," *J. Acoust. Soc. Am.*, vol. 128, no. 4, pp. 1700–1711, Jul. 2010.

[43] A. V. Mezheritsky, "Elastic, dielectric, and piezoelectric losses in piezoceramics: How it works all together," *IEEE Trans. Ultrason., Ferroelect., Freq. Control*, vol. 51, pp. 1582–1592, Jun 2004.

[44] L. Pardo, M. Algueró, and K. Brebøl, "Resonance modes in the standard characterization of ferro-piezoceramic samples: A discussion based on modelling by finite element analysis," *Ferroelect.*, vol. 336, no. 1, pp. 181–190, 2006.

[45] J. Zheng, S. Takahashi, S. Yoshikawa, K. Uchino, and J. De Vries, "Heat generation in multilayer piezoelectric actuators," *J. Am. Ceram. Soc.*, vol. 79, no. 12, pp. 3193–3198, Dec. 1996.

[46] M. S. Senousy, R. K. N. D. Rajapakse, D. Mumford, and M. S. Gadala, "Self-heat generation in piezoelectric stack actuators used in fuel injectors," *Smart Mater. Struct.*, vol. 18, no. 045008, Mar. 2009.

[47] A. Ochi, S. Takahashi, and S. Tagami, "Temperature characteristics for multilayer piezoelectric ceramic actuator," *Jpn. J. Appl. Phys.*, vol. 24, no. 209, pp. 209–212.

[48] H.-W. Joo, C.-H. Lee, J.-S. Rho, and H.-K. Jung, "Analysis of temperature rise for piezoelectric transformer using finite-element method," *IEEE Trans. Ultrason., Ferroelect., Freq. Control*, vol. 53, no. 8, pp. 1449–1457, Aug. 2006.

[49] J. Hu, "Analyses of the temperature field in a bar-shaped piezoelectric transformer operating in longitudinal vibration mode," *IEEE Trans. Ultrason., Ferroelect., Freq. Control*, vol. 50, no. 6, pp. 594–600, Jun. 2003.

[50] J. Hu, Y. Fuda, T. Yoshida *et al.*, "A study on the rectangular-bar-shaped multilayer piezoelectric transformer using length extensional vibration mode," *Jpn. J. Appl. Phys.*, vol. 38, no. 3208, pp. 3208–3212, 1999.

[51] M. Stewart and M. G. Cain, "Measurement and modelling of self-heating in piezoelectric materials and devices," in *Characterisation of ferroelectric bulk materials and thin films*, M. G. Cain, Ed., 2014.

Article 1

M. Wild, K. Hjerlmervik, L. Hoff and M. Bring, "Characterising piezoelectric material parameters through a 3D FEM and optimisation algorithm," in OCEANS 2017 - Aberdeen, pp. 1-5, IEEE, 2017, doi: 10.1109/OCEANSE.2017.8084983

Papers 1, 2, 4 and 5 are omitted from online publication due to publishers restrictions.

Article 2

M. Wild, M. Bring, L. Hoff and K. Hjerlmervik, "Characterization of Piezoelectric Material Parameters Through a Global Optimization Algorithm,", IEEE Journal of Oceanic Engineering, pp. 1-9,, 2019, doi: 10.1109/JOE.2018.2882262

Papers 1, 2, 4 and 5 are omitted from online publication due to publishers restrictions.

Article 3

M. Wild, M. Bring, E. Halvorsen, L. Hoff and K. Hjerlmervik, "The challenge of distinguishing mechanical, electrical and piezoelectric losses," Journal of Acoustical Society of America, 144(4), pp. 2128-2134, 2018, doi: 10.1121/1.5057443

The challenge of distinguishing mechanical, electrical and piezoelectric losses

Marcus Wild,[1,a)] Martin Bring,[2] Einar Halvorsen,[1] Lars Hoff,[1] and Karina Hjelmervik[1]
[1]*Faculty of Technology, Natural Sciences and Maritime Sciences, University of South-Eastern Norway, Campus Vestfold, Raveien 215, Borre 3184, Norway*
[2]*Subsea Division, Kongsberg Maritime, Strandpromenaden 50, Horten 3183, Norway*

(Received 15 May 2018; revised 30 August 2018; accepted 14 September 2018; published online 12 October 2018)

Understanding the energy loss in piezoelectric materials is of significant importance for manufacturers of acoustic transducers. The contributions to the power dissipation due to nonzero phase angles of the mechanical, electrical, and piezoelectric constants can be separated in the expression for power dissipation density. However, this division into separate contributions depends on the piezoelectric constitutive equation form used. Thus, it is problematic to identify any of the three terms with a specific physical domain, electric or mechanical, or to a coupling as is common in the discussion of loss in piezoelectric materials. Therefore, assumptions on the phase of the material constants based on this distinction could be erroneous and lead to incorrect piezoelectric models. This study demonstrates the challenge of distinguishing mechanical, electrical, and piezoelectric losses by investigating the power dissipation density and its contributions in a piezoelectric rod for all four piezoelectric constitutive equation forms. © *2018 Acoustical Society of America*.
https://doi.org/10.1121/1.5057443

[WM] Pages: 2128–2134

I. INTRODUCTION

Understanding loss in piezoelectric materials and having the ability to model the effects these mechanisms have on the behaviour of the material is of significant importance to acoustic transducer manufacturers. Energy loss in piezoelectric materials, the active part of the transducer, affects important characteristics of the transducer such as the bandwidth or the amount of heat generated. It is therefore beneficial to manufacturers to be able to include the effects of energy loss in piezoelectric models in the design phase. In this paper, the effect the imaginary terms of the material constants, commonly known as loss tangents, of a piezoelectric rod have on the power dissipation is quantified. This analysis is performed using the four common piezoelectric constitutive equation forms, the g-, d-, e-, and h-forms.

The power dissipation within a piezoelectric material originates from physical microscopic energy loss mechanisms associated with lattice deformation, domain, and grain effects.[1] Macroscopically, the net effect of these physical mechanisms is modeled in different ways. For ultrasound transducer design, it is common to use the mechanical quality factor Q_m, which is related to the sharpness of the resonance peak, and the dielectric loss $\tan(\delta)$ as a means of representing energy loss in these materials.[2–4] Holland[5] introduced the complex representation of the material constants in the piezoelectric constitutive equations. Under Holland's notation, the material constants in the strain-charge form, also known as the d-form of the piezoelectric constitutive equations, are complex in order to introduce a phase lag between the mechanical and electrical fields, a valid approximation for low losses and narrow frequency bands. In this representation, a nonzero phase in the mechanical, dielectric, and piezoelectric constants gives rise to loss terms that are conventionally named the mechanical, dielectric, and piezoelectric loss.[6–8] This terminology is now in common use in the literature considering characterisation of piezoelectric materials. Indeed, one-dimensional (1D) equivalent circuits such as the Krimholtz-Leedom-Matthaei (KLM) and Mason model can easily be implemented with complex material constants and so these parameters can be characterised using similar methods to those defined by the IEEE Standard on Piezoelectricity.[7–9] Finite-Element-Method (FEM)-based characterisation, which fits the modelled impedance curve to the measured impedance curve, has also been developed to take complex material constants into account.[10–12]

Whilst the characterisation methods mentioned above take into account all three loss terms, it is also habitual in practice and in research to ignore the imaginary part of the piezoelectric constants.[13–15] The reasoning behind this assumption is that the effect of the piezoelectric loss term is negligible compared to the mechanical and electrical loss terms. On the other hand, studies have shown that the piezoelectric loss term can in fact have a significant contribution, especially with regards to power dissipation.[6,7] To this end, Uchino *et al.*[16] have developed characterisation methods and equivalent circuits which include all three loss terms. Uchino and Hirose[6] distinguish between the intensive losses, the losses for the d-form material constants, and extensive losses, the losses for the h-form, also known as the stress-voltage form, material constants. They conclude that the intensive mechanical loss is the dominant loss mechanism at resonance, whilst the intensive dielectric loss is dominant outside of resonance for a plate. Similar

a)Electronic mail: marcus.wild@usn.no

conclusions are stated in other studies dealing with losses in transducers.[17–19]

Uchino and Hirose[6] consider the individual extensive loss terms to have real physical meaning. Similar statements that attach a physical mechanism to the complex representation of losses are regularly seen across the literature.[11,20,21] Sherrit and Mukherjee[22] specify that a distinction should be made between macroscopic behaviour of the piezoelectric material, described by the complex material constants, and the microscopic behaviour in the material.

A generalised Poynting vector can be defined as the sum of the electrical and mechanical energy flux in a piezoelectric material.[5,23] It has been used to explicitly quantify the contribution the various material constants have towards the power dissipation in a piezoelectric material.[24,25] Thomas *et al.*[24] use complex material constants to model the power dissipation in a length extensional piezoelectric slab. The power dissipation is then separated out into a mechanical, electrical, and piezoelectric contribution. Mezheritsky[25] derives the same expressions for the three contributions and notably demonstrates that the piezoelectric contribution to the power dissipation can be negative over parts of the frequency spectrum.

This study aims to gain a deeper understanding into the effect the various complex material constants have on the power dissipation in a piezoelectric material. However, rather than limiting the study to one piezoelectric constitutive form, the contributions from the complex material constants for the four common forms will be compared. In order to achieve this, a fully characterised piezoelectric rod will be simulated using the 1D Mason model. The output from the 1D model will be used as the input into the generalised Poynting vector which will give four different expressions for the power dissipation density in a piezoelectric rod, one for each formulation of the constitutive equations. From this, the total power dissipation can be calculated as a function of frequency.

II. THEORY

A. Piezoelectric equations for a length extensional rod

The g-form, also known as the strain-voltage form, piezoelectric constitutive equations are given by

$$\begin{aligned} S_p &= s^D_{pq} T_q + g_{pm} D_m, \\ E_m &= -g_{pm} T_p + \beta^T_{mn} D_n, \end{aligned} \tag{1}$$

where S is the strain tensor, T is the stress tensor, E is the electric field tensor, D is the electric displacement tensor, s^D is the elastic compliance tensor at constant electric displacement field, g is the piezoelectric constant tensor, β^T is the electric impermittivity tensor at constant stress, and m, n, p, q are the tensor indices. The temperature dependence of the piezoelectric constitutive equations is carried by these material constants. These material constants are complex in order to represent the phase lags between the field tensors as defined by Holland.[5]

For the case of a long rod with ∞m symmetry, electrodes on either end and lateral dimensions smaller than the longitudinal wavelength as shown in Fig. 1, $T_1 = T_2 = 0$, $E_1 = E_2 = 0$, $D_1 = D_2 = 0$, and $dD_3/dx_3 = 0$ at resonance.[26] In addition, the shear stress and strain are omitted. Given these assumptions, the g-form of the piezoelectric constitutive equations in Eq. (1) is conveniently simplified to a 1D problem where

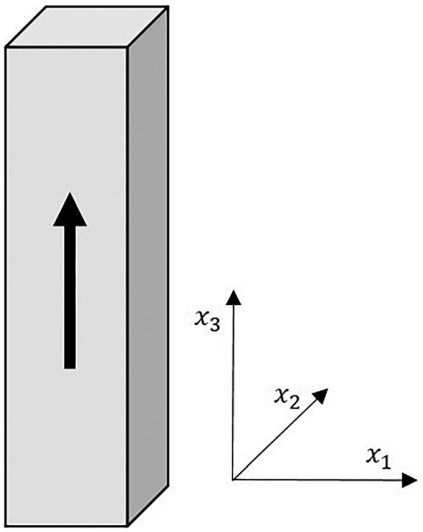

FIG. 1. A piezoelectric rod polarised in the direction of the bold arrow.

$$\begin{aligned} S_3 &= s^D_{33} T_3 + g_{33} D_3, \\ E_3 &= -g_{33} T_3 + \beta^T_{33} D_3. \end{aligned} \tag{2}$$

The d-, e-, and h-forms, also known as the strain-charge, stress-charge, and stress-voltage forms of the piezoelectric constitutive equations can then derived from the g-form [Eq. (2)] so that

$$\begin{aligned} S_3 &= s^E_{33} T_3 + d_{33} E_3, \\ D_3 &= d_{33} T_3 + \varepsilon^T_{33} E_3, \end{aligned} \tag{3}$$

$$\begin{aligned} T_3 &= c^E_{\text{eff}} S_3 - e_{\text{eff}} E_3, \\ D_3 &= e_{\text{eff}} S_3 + \varepsilon^S_{\text{eff}} E_3, \end{aligned} \tag{4}$$

$$\begin{aligned} T_3 &= c^D_{\text{eff}} S_3 - h_{\text{eff}} D_3, \\ E_3 &= -h_{\text{eff}} S_3 + \beta^S_{\text{eff}} D_3. \end{aligned} \tag{5}$$

The material properties derived from the g-form are listed in Table I. The 33 subscripts indicate the (3, 3) tensor indices. This is the case for the d-form given our assumptions and the ∞m symmetry of the material. The material

TABLE I. List of the material parameters for the piezoelectric rod used in this study.

Material Constants	Value
s^D_{33} [$10^{-12} \times \text{m}^2/\text{N}$]	$7.80 - 0.31j$
β^T_{33} [$10^8 \times \text{m/F}$]	$1.16 + 0.0033j$
g_{33} [$10^{-2} \times \text{Vm/N}$]	$2.34 - 0.02j$
ρ [kg/m^3]	7500

constants with "eff" as subscript are 1D effective material constants and do not represent the actual (3, 3) value of the material tensor.

B. Generalised Poynting vector

The generalised Poynting vector Σ for a piezoelectric material is given by

$$\mathbf{\Sigma} = \frac{1}{2}(\mathbf{E} \times \mathbf{H}^* - \mathbf{T} \cdot \mathbf{u}^*), \tag{6}$$

where $\mathbf{H}$ is the magnetic field, $\mathbf{u}$ is the particle velocity, * marks the complex conjugate, and $\cdot$ is the inner product.

The power dissipation density for piezoelectric materials can be derived from Eq. (6) as[5]

$$P = \frac{1}{2}\omega \mathrm{Im}(\mathbf{E} \cdot \mathbf{D}^* + \mathbf{T} : \mathbf{S}^*), \tag{7}$$

where P is the power dissipation density, ω is the angular frequency and : is the inner product of second order tensors. Using 1D assumptions for the length extensional mode of a piezoelectric rod, Eq. (7) simplifies to

$$P = \frac{1}{2}\omega \mathrm{Im}\left(E_3 D_3^* + T_3 S_3^*\right). \tag{8}$$

Inserting the expressions for D_3, S_3, T_3, and E_3 from the g-, d-, e-, and h-form piezoelectric equations into Eq. (8) yields four different expressions for the power dissipation density consisting of three terms. In the case of the g-form, this yields

$$P = P_{g,1} + P_{g,2} + P_{g,3}, \tag{9}$$

where

$$\begin{aligned}
P_{g,1} &= \frac{1}{2}\omega \mathrm{Im}\left(T_3 s_{33}^{D*} T_3^*\right) = -\frac{1}{2}\omega |T_3|^2 \mathrm{Im}\left(s_{33}^D\right), \\
P_{g,2} &= \frac{1}{2}\omega \mathrm{Im}\left(D_3 \beta_{33}^T D_3^*\right) = \frac{1}{2}\omega |D_3|^2 \mathrm{Im}\left(\beta_{33}^T\right), \\
P_{g,3} &= \frac{1}{2}\omega \mathrm{Im}\left(-T_3 g_{33} D_3^* + T_3 g_{33}^* D_3^*\right) \\
&= -\omega(\mathrm{Re}(T_3)\mathrm{Re}(D_3) + \mathrm{Im}(T_3)\mathrm{Im}(D_3))\mathrm{Im}(g_{33}).
\end{aligned}$$

For the d-form,

$$P = P_{d,1} + P_{d,2} + P_{d,3}, \tag{10}$$

where

$$\begin{aligned}
P_{d,1} &= -\frac{1}{2}\omega |T_3|^2 \mathrm{Im}\left(s_{33}^E\right), \\
P_{d,2} &= -\frac{1}{2}\omega |E_3|^2 \mathrm{Im}\left(\varepsilon_{33}^T\right), \\
P_{d,3} &= -\omega(\mathrm{Re}(E_3)\mathrm{Re}(T_3) + \mathrm{Im}(E_3)\mathrm{Im}(T_3))\mathrm{Im}(d_{33}).
\end{aligned}$$

For the e-form

$$P = P_{e,1} + P_{e,2} + P_{e,3}, \tag{11}$$

where

$$\begin{aligned}
P_{e,1} &= \frac{1}{2}\omega |S_3|^2 \mathrm{Im}\left(c_{\mathrm{eff}}^E\right), \\
P_{e,2} &= -\frac{1}{2}\omega |E_3|^2 \mathrm{Im}\left(\varepsilon_{\mathrm{eff}}^S\right), \\
P_{e,3} &= -\omega\left(\mathrm{Re}(E_3)\mathrm{Re}(S_3) + \mathrm{Im}(E_3)\mathrm{Im}(S_3)\right)\mathrm{Im}(e_{\mathrm{eff}}).
\end{aligned}$$

For the h-form,

$$P = P_{h,1} + P_{h,2} + P_{h,3}, \tag{12}$$

where

$$\begin{aligned}
P_{h,1} &= \frac{1}{2}\omega |S_3|^2 \mathrm{Im}\left(c_{\mathrm{eff}}^D\right), \\
P_{h,2} &= \frac{1}{2}\omega |D_3|^2 \mathrm{Im}\left(\beta_{\mathrm{eff}}^S\right), \\
P_{h,3} &= -\omega\left(\mathrm{Re}(S_3)\mathrm{Re}(D_3) + \mathrm{Im}(S_3)\mathrm{Im}(D_3)\right)\mathrm{Im}(h_{\mathrm{eff}}).
\end{aligned}$$

For all four forms, the power dissipation density has been split into three terms. $P_{s,1}$, where s is the form used, which only consists of mechanical terms in all four forms, has previously been interpreted as the mechanical contribution to the total power dissipation density.[6,24,25] Using the same logic, $P_{s,2}$, which only consists of electrical terms, could be interpreted as the electrical contribution, and $P_{s,3}$, which only consists of piezoelectric terms, could be interpreted as the piezoelectric contribution to the total power dissipation density.

The total power dissipation Ω in the piezoelectric rod and its contributing terms are given by

$$\Omega = A \int_0^L P \mathrm{d}x_3 = \Omega_{s,1} + \Omega_{s,3} + \Omega_{s,3}, \tag{13}$$

where A is the cross sectional area of the piezoelectric rod, L is the length of the piezoelectric rod and

$$\Omega_{s,n} = A \int_0^L P_{s,n} \mathrm{d}x_3, \tag{14}$$

where $n = 1, 2, 3$. It follows that $\Omega_{s,1}$, $\Omega_{s,2}$, and $\Omega_{s,3}$ are interpreted as the mechanical, electrical, and piezoelectric contribution to the total power dissipation in the piezoelectric rod. It is important to note that although there is a requirement for the total power dissipation density and power dissipation to be positive, this requirement does not apply to the individual contributions. Indeed, $\Omega_{s,3}$ has been shown to be negative in previous studies.[25]

III. METHOD

To illustrate the effect the loss terms exhibit on the power dissipation in a piezoelectric material, the 1D Mason model, shown in Fig. 2, was used to calculate the behaviour of a piezoelectric rod at the fundamental resonance of the length extensional mode. The circuit parameters are given by

$$\begin{aligned}
&C_0 = \varepsilon_{33}^S A/L, \\
&N_c = A d_{33}/L s_{33}^E, \quad Z_a = j\rho c A \tan(kL/2), \\
&c = 1/\sqrt{s_{33}^D \rho}, \quad Z_b = -j\rho c A/\sin(kL),
\end{aligned} \tag{15}$$

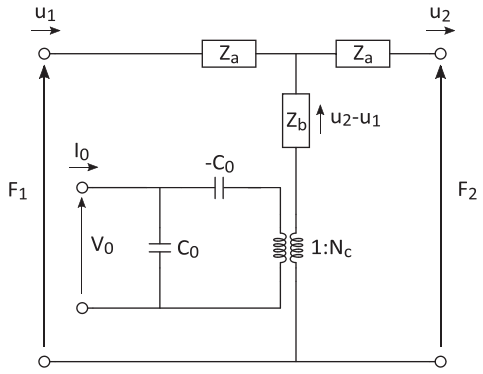

FIG. 2. Mason 3-port equivalent circuit for the mechanical motion and electrical current of a piezoelectric rod (Ref. 26). u_1, F_1, u_2, and F_2 are the velocity and force on either end of the rod, and I_0 and V_0 the current and voltage at the electrical port.

where L is the length of the rod, A is the cross sectional area of the rod, c is the speed of sound, $k = \omega/c = 2\pi/\lambda$ is the wave number, with λ the wavelength, and ρ is the density of the piezoelectric material.

It was assumed that there are no external forces acting on the rod ($F_1 = F_2 = 0$) and that the electrodes at the terminals were of negligible thickness. The driving voltage in the model is arbitrarily set to $1V_p$ as this value does not affect the comparisons in this linear analysis. The material constants of EDO EC-69, listed in Table II from a full characterisation study by Sabat *et al.*,[27] were used as the input into the model. The rod has dimensions 3 mm × 3 mm × 20 mm.

Using the 1D Mason model and the characterised material constants, the power dissipation density of the piezoelectric rod as a function of position in the rod and frequency can be calculated. This is achieved by using the expression for power dissipation density as shown in Eq. (7). The three contributing terms for all four forms [Eqs. (9)–(12)] are calculated at the resonance and antiresonance frequency in order to determine the importance of each quantity. The same procedure is followed for the power dissipation as a function of frequency [Eqs. (13) and (14)].

TABLE II. List of the derived material constants for the different forms of the piezoelectric constitutive equations.

Material Constants	Material Property	Transform from g-form
s_{33}^E	Elastic compliance at constant electric field	$s_{33}^D + \frac{g_{33}^2}{\beta_{33}^T}$
ε_{33}^T	Electric impermittivity at constant stress	$\frac{1}{\beta_{33}^T}$
d_{33}	Piezoelectric constant	$\frac{g_{33}}{\beta_{33}^T}$
c_{eff}^E	Elastic stiffness at constant electric field	$\frac{1}{s_{33}^E}$
$\varepsilon_{\text{eff}}^S$	Electric permittivity at constant strain	$\varepsilon_{33}^T - \frac{d_{33}^2}{s_{33}^E}$
e_{eff}	Piezoelectric constant	$\frac{d_{33}}{s_{33}^E}$
c_{eff}^D	Elastic stiffness at constant electric displacement field	$\frac{1}{s_{33}^D}$
β_{eff}^S	Electric impermittivity at constant strain	$\beta_{33}^T + \frac{g_{33}^2}{s_{33}^D}$
h_{eff}	Piezoelectric constant	$\frac{g_{33}}{s_{33}^D}$

IV. RESULTS

The contributions from the terms detailed in Eqs. (9)–(12) to the total power dissipation density are shown in Fig. 3 at the resonance frequency and in Fig. 4 at the antiresonance frequency. The contributions have been separated into $P_{s,1}$, $P_{s,2}$, and $P_{s,3}$, where s is the form of the piezoelectric constitutive equation. These contributions are different depending on the form used, even though the total contribution is identical for a given frequency.

At resonance, for all four forms, $P_{s,1}$, the term associated with mechanical fields is the dominating term which contributes the most to the total power dissipation density P. $P_{s,2}$, the term associated with the electrical fields, contributes the least to P in all cases. $P_{s,3}$, the term associated with a mixture of electrical and mechanical fields, is mostly negligible except for the h-form, where it has a significant negative contribution to the total power dissipation density. It is important to note that in the d-, e-, and h-form, $P_{s,3}$ has a negative contribution at least for part of the piezoelectric rod, whereas $P_{s,1}$ and $P_{s,2}$ are always positive. The sign of $P_{s,1}$ and $P_{s,2}$ is completely determined by the sign of the imaginary part of the mechanical and electrical material constants, whereas the sign of $P_{s,3}$ is also determined by the phase differences between the electrical and mechanical fields.

At the antiresonance frequency, $P_{s,1}$ is still the dominating term for all four forms, especially in the g- and h-forms (where $P_{g,1} \simeq P_{h,1} \simeq P$). $P_{d,3}$, $P_{e,3}$, $P_{d,2}$, and $P_{e,2}$ account for a significant portion of the total power dissipation density. Indeed, $P_{e,2} + P_{e,3} \simeq P_{e,1}$.

The normalised contributions as a function of frequency from the terms detailed in Eqs. (14) to the total power dissipation are shown in Fig. 5. The contributions have been separated into $\Omega_{s,1}$, $\Omega_{s,2}$, and $\Omega_{s,3}$ and normalised with respect to Ω, where s is the form of the piezoelectric constitutive equation. The interplay between the various terms changes as a function of frequency and with each form. Most notably, $\Omega_{s,3}$ changes sign near the resonance or antiresonance frequency for all four forms. In the d- and e-form, the frequency at which $\Omega_{s,3}$ changes sign, the resonance frequency, is also the frequency at which $\Omega_{s,2}$ is at its minimum and is approximately null. Consequently, at the resonance frequency, $\Omega_{s,1} \simeq \Omega$. The same conclusions can be drawn for the g- and h-form at the antiresonance frequency. In other parts of the frequency spectrum, Ω is not dominated by one contribution but more evenly distributed between two or more contributions. For the g-form at the resonance frequency, $\Omega_{g,1}$, $\Omega_{g,2}$, and $\Omega_{g,3}$ account for 80%, 3%, and 17% of the total power dissipation, respectively. At the antiresonance frequency in the e-form, $\Omega_{e,1}$, $\Omega_{e,2}$, and $\Omega_{e,3}$ account for 50%, 10%, and 40% of the total power dissipation, respectively.

A three-dimensional (3D) FEM model of the same piezoelectric material and shape was simulated using COMSOL in order to check the validity of the results from the 1D

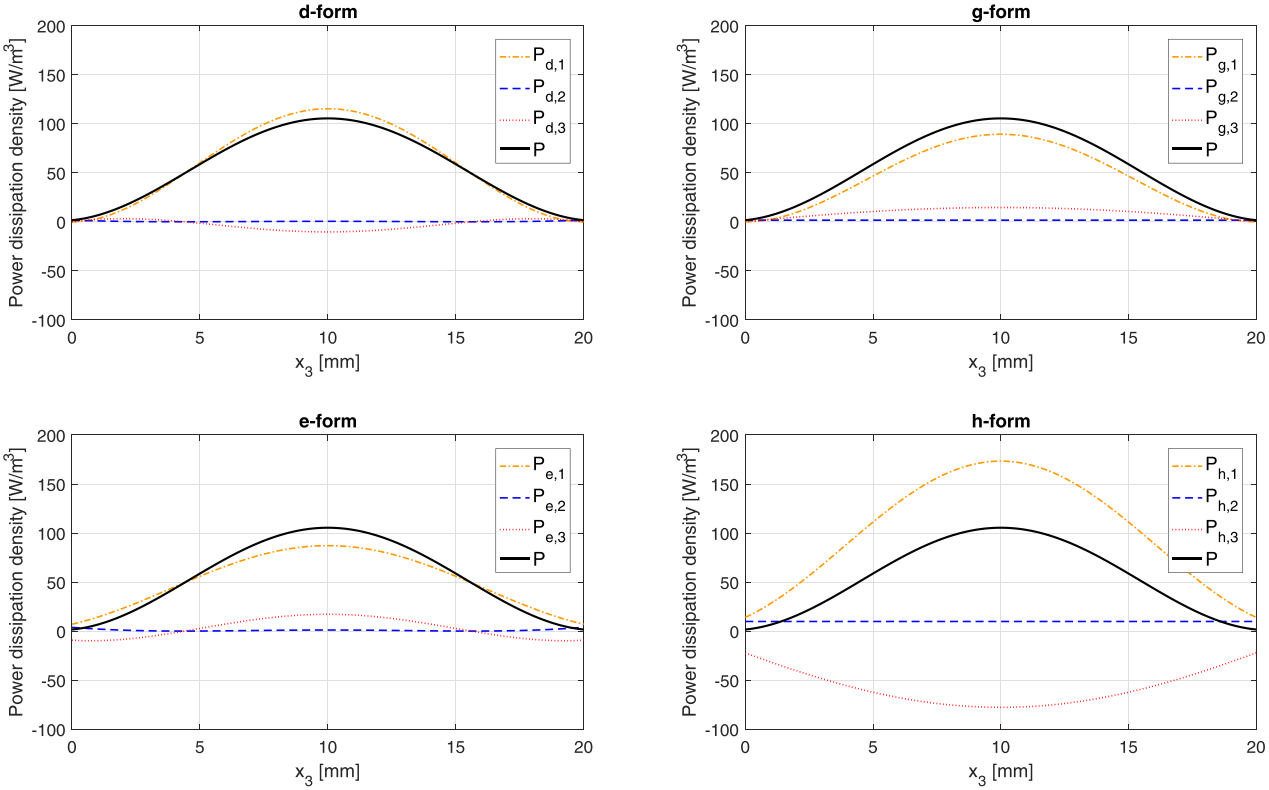

FIG. 3. The power dissipation density, P, in the piezoelectric rod and its three contributions as a function of x_3 at resonance for all four forms.

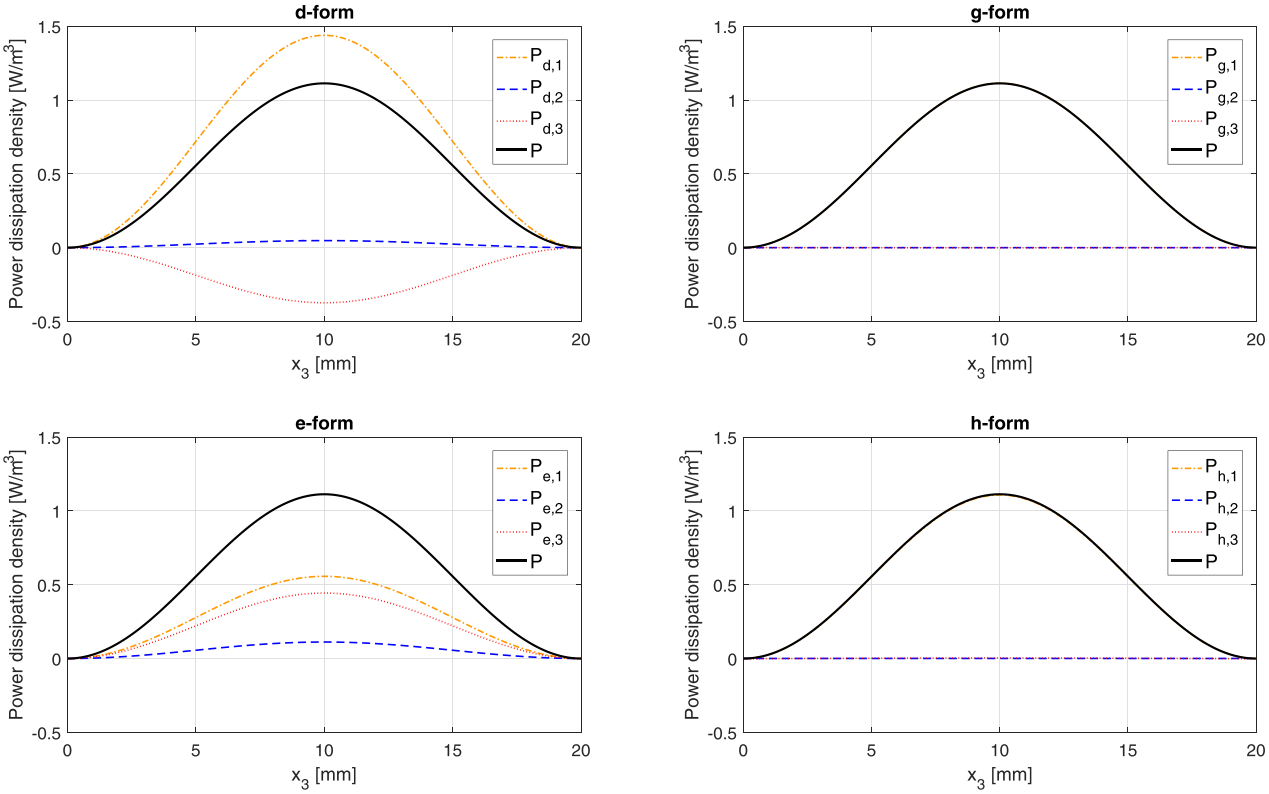

FIG. 4. The power dissipation density, P, in a piezoelectric rod and its three contributions as a function of x_3 at antiresonance for all four forms.

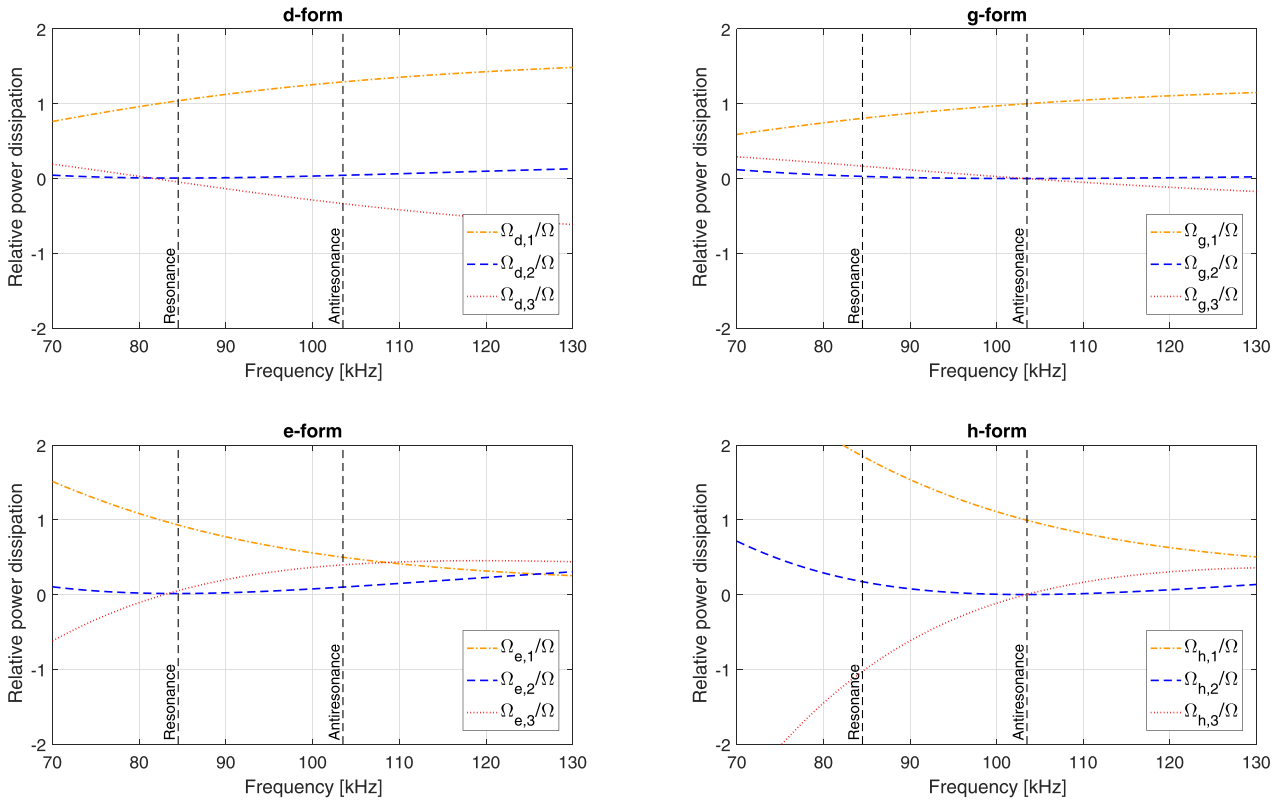

FIG. 5. The three normalised contributions to the total power dissipation as a function of frequency for all four forms. The contributions are normalised with respect to the total power dissipation, Ω. The resonance and antiresonance frequency are annotated.

Mason model. There is excellent agreement between the 1D and 3D model at the frequency of interest with errors low enough to have no effect on the conclusions.[28]

V. DISCUSSION

Depending on the piezoelectric constitutive equation form used, the contributions to the power dissipation density from the mechanical, electrical, and piezoelectric constants are different at resonance and antiresonance (Figs. 3 and 4). Most notably, the contributions from the piezoelectric constants can be negative over certain areas of the rod. This is also the case for the contribution from $\Omega_{s,3}$ to the total power dissipation in the rod as a function of frequency (Fig. 5). For all four forms, the contributions from the piezoelectric constants are negative over parts of the spectrum. On this point, there is agreement with the Mezheritsky[25] analysis on the contribution from the piezoelectric constant.

Due to the different nature of the three contributions to the power dissipation density for each form, attaching any physical meaning to the individual terms, and therefore to the imaginary part of the material constants, is not recommended. The results show that in various forms, $P_{s,1}$, which has been interpreted as the mechanical power dissipation density in other studies, can be larger than the total power dissipation density in the rod. Clearly this is not consistent when considering power dissipation and cannot meaningfully be attributed to a physical mechanism. Similarly, $P_{s,3}$, which has been interpreted as the power dissipation density as a result of imperfect energy conversion between the mechanical and electrical domain, is negative over parts of the frequency spectrum.

The phenomenological description of piezoelectric materials requires complex material constants to model macroscopic behaviour of the energy loss in the material. However, in reality, the imaginary parts of the material constants have a complicated relationship with the microscopic sources of these energy loss mechanisms. Sherrit and Mukherjee[22] resort to more complicated phenomenological models in order to relate the microscopic sources of energy loss to the macroscopic behaviour.

The practical implication of not attaching any physical meaning to these contributions is to reduce the amount of assumptions based on physical interpretations of the energy loss terms in the material constants when modeling piezoelectric materials. For example, the common perception that the imaginary part of the piezoelectric constant, commonly known as the piezoelectric loss, is negligible based on the limited effect of the energy loss due to imperfect energy conversion between the mechanical and electrical domain does not hold based on the results of this study. In all four forms, $\Omega_{s,3}$ clearly has more of an effect on the total power dissipation in the rod than $\Omega_{s,2}$, which is commonly associated with dielectric loss (Fig. 5). Furthermore, assuming that only mechanical energy is dissipated at resonance does not always hold depending on the form used. Indeed, in the g- and h-form in Fig. 5, $\Omega_{s,3}$ contributes a significant amount to the total power dissipation Ω (approximately 17% in the case of the g-form). Ignoring these effects could lead to

erroneous piezoelectric models, especially when considering heat generation.

Although the findings from this study are partly based on effective material parameters in the e- and h-form, the conclusions still hold when only considering the true material parameters in the d- and g-forms. Only the power dissipation as a result of fields in the x_3-direction were included as this study was conducted with a 1D model. This study can also be conducted in 3D using FEM in order to include the lateral fields; however, these have a minimal effect on the total power dissipation at the fundamental resonance in the length extensional mode of a piezoelectric rod. The behaviour of only one material with a specific shape was analysed in this work. Determining whether the particular assumptions that apply to this shape and material, such as the dominance of the imaginary parts of the mechanical constants in the d- and e-form at resonance, can be generalised to other materials and shapes would require a more comprehensive study.

VI. CONCLUSION

The power dissipation density and power dissipation as a result of the complex representation of material constants was calculated in a piezoelectric rod using the 1D Mason model at the fundamental length extensional resonance for all four forms of the piezoelectric constitutive equations. Although the total power dissipation density and total power dissipation remain the same for all piezoelectric constitutive forms, the contributing terms vary significantly. There is therefore no means of extracting a unique mechanical, electrical, and piezoelectric contribution with any individual physical meaning from this phenomenological model. Hence, the phase of the material constants does not reflect the energy loss from one specific physical loss mechanism, but rather a complicated combination of a number of these physical loss mechanisms. Therefore, this study has demonstrated that any assumptions on the imaginary part of the material constants based on real mechanical, electrical, and piezoelectric power dissipation mechanisms does not hold in this type of phenomenological model.

ACKNOWLEDGMENT

This work was supported by the Research Council of Norway, Grant Nos. 237887 and 273248.

[1]G. Lie, S. Zhang, W. Jiang, and W. Cao, "Losses in ferroelectric materials," Mater. Sci. and Eng. R **89**, 1–48 (2015).
[2]H. J. Lee and S. Zhang, "Design of low-loss 1-3 piezoelectric composites for high-power transducer applications," IEEE Trans. Ultrason. Ferroelectr. Freq. Control **59**(9), 1969–1975 (2012).
[3]G. Whitworth, "Discussion of one-D piezoelectric transducer models with loss," IEEE Trans. Ultrason. Ferroelectr. Freq. Control **48**, 844–846 (2001).
[4]F. J. Arnold, M. S. Gonçalves, F. R. Massaro, Jr., and P. S. Martins, "Evaluation of mechanical losses in piezoelectric plates using genetic algorithm," in *Proceedings of the 2015 ICU International Congress on Ultrasonics*, Metz, France (May 10–14, 2015), pp. 905–908.
[5]R. Holland, "Representation of dielectric, elastic, and piezoelectric losses by complex coefficients," IEEE Trans. Sonics Ultrason. **14**(1), 18–20 (1967).
[6]K. Uchino and S. Hirose, "Loss mechanisms in piezoelectrics: How to measure different losses separately," IEEE Trans. Ultrason. Ferroelectr. Freq. Control **48**(1), 307–321 (2001).
[7]S. Sherrit, S. P. Leary, B. P. Dolgin, and Y. Bar-Cohen, "Comparison of the Mason and KLM equivalent circuits for piezoelectric resonators in the thickness mode," in *Proceedings of the IEEE Ultrasonics Symposium*, Lake Tahoe, NV (October 17–19, 1999), Vol. 2, pp. 921–926.
[8]X. Dong, M. Majzoubi, M. Choi, Y. Ma, M. Hu, L. Jin, Z. Xu, and K. Uchino, "A new equivalent circuit for piezoelectrics with three losses and external loads," Sens. Actuators A **256**, 77–83 (2017).
[9]C. Joh, J. Kim, and Y. Roh, "Determination of the complex material constants of PMN–28%PT piezoelectric single crystals," Smart Mater. Struct. **22**, 125027 (2013).
[10]C. Y. Kiyono, N. Peréz, and E. C. N. Silva, "Determination of full piezoelectric complex parameters using gradient-based optimization algorithm," Smart Mater. Struct. **25**, 025019 (2016).
[11]T. Lahmer, M. Kaltenbacher, B. Kaltenbacher, R. Lerch, and E. Leder, "FEM-based determination of real and complex elastic, dielectric, and piezoelectric moduli in piezoceramic materials," IEEE Trans. Ultrason. Ferroelectr. Freq. Control **55**(2), 465–475 (2008).
[12]N. Pérez, F. Buiochi, M. A. Brizzotti Andrade, and J. C. Adamowski, "Numerical characterization of piezoceramics using resonance curves," Materials **9**(2), 71 (2016).
[13]L. P. Tran-Huu-Hue, F. Levassort, N. Felix, D. Danjanovic, W. Wolny, and M. Lethiecq, "Comparison of several methods to characterise the high frequency behaviour of piezoelectric ceramics for transducer applications," Ultrasonics **38**, 219–223 (2000).
[14]M. Lethiecq, L. P. Tran-Huu-Hue, F. Patat, and L. Pourcelot, "Measurement of losses in five piezoelectric ceramics between 2 and 50 MHz," IEEE Trans. Ultrason., Ferroelect., Freq. Control **40**, 232–237 (1993).
[15]V. Loyau, Y.-P. Liu, and F. Costa, "Analyses of the heat dissipated by losses in a piezoelectric transformer," IEEE Trans. Ultrason. Ferroelectr. Freq. Control **56**, 1745–1752 (2009).
[16]K. Uchino, Y. Zhuang, and S. O. Seyit, "Loss determination methodology for a piezoelectric ceramic: New phenomenological theory and experimental proposals," J. Adv. Dielectr. **1**, 17–31 (2011).
[17]D. Guyomar, N. Aurelie, L. Eyraud, and P. S. Martins, "Simulations of transducer behavior as a function of the frequency and the mechanical, dielectric and piezoelectric losses," in *Proceedings of the Tenth IEEE International Symposium, Applications of Ferroelectrics, ISAF'96*, East Brunswick, NJ (August 18–21, 1996), Vol. 1, pp. 365–372.
[18]H. J. Lee, S. Zhang, Y. Bar-Cohen, and S. Sherrit, "High temperature, high power piezoelectric composite transducers," Sensors **14**(8), 14526–14552 (2014).
[19]M. S. Senousy, R. K. N. D. Rajapakse, D. Mumford, and M. S. Gadala, "Self-heat generation in piezoelectric stack actuators used in fuel injectors," Smart Mater. Struct. **18**, 045008 (2009).
[20]A. Ochi, S. Takahashi, and S. Tagami, "Temperature characteristics for multilayer piezoelectric ceramic actuator," Jpn. J. Appl. Phys. **24**, 209–212 (1985).
[21]H. Wang, Q. Zhang, and L. E. Cross, "A high sensitivity, phase sensitive d33 meter for complex piezoelectric constant measurement," Jpn. J. Appl. Phys. **32**(9A), L1281–L1283 (1993).
[22]S. Sherrit and B. K. Mukherjee, "The use of complex material constants to model the dynamic response of piezoelectric materials," in *Proceedings of the IEEE Ultrasonics Symposium*, Sendai, Japan (October 5–8, 1998), Vol. 2, pp. 633–640.
[23]B. A. Auld, *Acoustic Fields and Waves in Solids*, 2nd ed. (Wiley, New York, 1973). Vol. 1, Chap. 8, p. 311.
[24]D. Thomas, D. D. Ebenezer, and S. M. Srinivasan, "Power dissipation and temperature distribution in piezoelectric ceramic slabs," J. Acoust. Soc. Am. **128**(4), 1700–1711 (2010).
[25]A. V. Mezheritsky, "Elastic, dielectric, and piezoelectric losses in piezoceramics: How it works all together," IEEE Trans. Ultrason. Ferroelectr. Freq. Control **51**, 695–707 (2004).
[26]J. L. Butler and C. H. Sherman, *Transducers and Arrays for Underwater Sound*, 2nd ed. (Springer, New York, 2016), Chap. 3, pp. 123–124.
[27]R. G. Sabat, B. K. Mukherjee, W. Ren, and G. Yang, "Temperature dependence of the complete material coefficients matrix of soft and hard doped piezoelectric lead zirconate titanate ceramics," J. Appl. Phys. **101**, 064111 (2007).
[28]See supplementary material at https://doi.org/10.1121/1.5057443 for comparison of results between the 1D and 3D model.

Article 4

M. Wild, M. Bring, L. Hoff and K. Hjerlmervik, "Comparison of two models for power dissipation and temperature in piezoelectric transducers," in 2018 IEEE International Ultrasonics Symposium (IUS), pp. 1-4, IEEE, 2018, doi: 10.1109/ULTSYM.2018.8580069

Papers 1, 2, 4 and 5 are omitted from online publication due to publishers restrictions.

Article 5

M. Wild, M. Bring, L. Hoff and K. Hjerlmervik, "Estimating the spatial temperature distribution in a piezoelectric rod," submitted to IEEE Transactions on ultrasonics, Ferroelectrics and frequency control, pp. 1-7, 2019

Papers 1, 2, 4 and 5 are omitted from online publication due to publishers restrictions.

Doctoral dissertation no. 38
2019
—

Heat generation in underwater transducers

Dissertation for the degree of PhD

—

Marcus Sebastian Wild

—

ISBN: 978-82-7860-380-2 (print)
ISBN: 978-82-7860-381-9 (online)

usn.no